NASA CONTRACTOR REPORT

NASA CR-444

NASA CR-444

PHOTOVISCOELASTICITY

by Ellis Harold Dill and Charless Fowlkes

Prepared under Grant No. NsG-401 *by*
UNIVERSITY OF WASHINGTON
Seattle, Wash.
for

NATIONAL AERONAUTICS AND SPACE ADMINISTRATION - WASHINGTON, D. C. - MAY 1966

NASA CR-444

PHOTOVISCOELASTICITY

By Ellis Harold Dill and Charless Fowlkes

Prepared under Grant No. NsG-401 by
UNIVERSITY OF WASHINGTON
Seattle, Wash.

for

NATIONAL AERONAUTICS AND SPACE ADMINISTRATION

For sale by the Clearinghouse for Federal Scientific and Technical Information
Springfield, Virginia 22151 – Price $1.45

ABSTRACT

This report provides a basis for the description of the mechanical and optical properties of birefringent, viscoelastic materials, and for the application of these materials in experimental stress analysis by photomechanics. The experimental procedure is applied to two plane stress problems. Preparation of the model, characterization of the material, and the test apparatus are also described.

TABLE OF CONTENTS

1. INTRODUCTION.

Many problems in structural engineering related to the structural integrity of solid propellants or the deformation of heated metal and ceramic structures can be reduced to the stress analysis of a linear viscoelastic material. The stress analysis of bodies with irregular boundaries is such a complicated mathematical problem that it is frequently more simple to determine the stress state by experiments upon a model. This report deals with the extension of the method of experimental stress analysis known as photoelasticity to viscoelastic materials.

The basic idea is to manufacture a model from a transparent, birefringent material and to determine the stress state of the model by observation of the fringe pattern which occurs when the model is placed between polaroids. In order to correlate the stress in the prototype with that of the model, the mechanical properties of the model and the prototype must be similar. Thus, the material of the model must, generally, be viscoelastic. Birefringent materials having the desired mechanical properties can be manufactured from high polymers.

The fringe pattern observed when birefringent materials are placed between polaroids is due to the dielectric properties of the material. The isoclinic and isochromatic fringe patterns give information about the dielectric

properties at any instant.

The dielectric properties of a birefringent, viscoelastic material at any instant depend upon the entire history of deformation. The fringe pattern changes with time, even when the stress or strain is constant.

The relation between dielectric properties and mechanical state can be inverted. Thus, the strain or stress at any instant depends on the entire history of dielectric properties. This means that it is necessary to have a complete time record of the history of isochromatic and isoclinic fringe patterns in order to gain information about the present value of the stress. This is the main difference between photoelastic and photoviscoelastic procedures.

The applications described in this report will be limited to quasi-static problems. It will be seen that photoviscoelasticity is a practical tool for engineering design.

2. VISCOELASTICITY.

2.1. Basic Equations.

In the following sections, some results from the classical theory of viscoelasticity are presented. The equations are limited to small displacements and quasi-static loads. The usual cartesian tensor indicial notation and summation convention are used in some places and standard scalar notation in others.

In rectangular cartesian coordinates, the equilibrium equations are

$$\partial_m \sigma_{km} + f_k = 0. \qquad (1)$$

The body force f_k will be negligible in the experiments. The σ_{km} are the components of the stress tensor which is symmetric. The symbol ∂_m will mean partial derivative with respect to the rectangular cartesian coordinate x^m, throughout the following discussion.

The components of the strain tensor ϵ_{km} are related to the displacement vector u_k by

$$\epsilon_{km} = \tfrac{1}{2} (\partial_k u_m + \partial_m u_k). \qquad (2)$$

In order to write the stress-strain relations it is convenient to introduce the deviatoric stress s_{km} and deviatoric strain e_{km} defined by

$$s_{km} = \sigma_{km} - 1/3\, \sigma_{rr}\, \delta_{km}, \qquad (3)$$

$$e_{km} = \epsilon_{km} - 1/3\ \epsilon_{rr}\ \delta_{km}. \qquad (4)$$

where δ_{km} denotes the Kronecker delta. Then, for an isotropic material

$$s_{km} = \int_o^t 2G(t-\tau)\ \dot{e}_{km}(\tau)\ d\tau, \qquad (5)$$

$$1/3\ \sigma_{rr} = \int_o^t K(t-\tau)\ \dot{\epsilon}_{rr}(\tau)\ d\tau. \qquad (6)$$

Where, the dot indicates the derivative with respect to the argument indicated.

The inverses of equations (5) and (6) are

$$2e_{km} = \int_o^t J(t-\tau)\ \dot{s}_{km}(\tau)\ d\tau, \qquad (7)$$

$$\epsilon_{rr} = \int_o^t 1/3\ B(t-\tau)\ \dot{\sigma}_{rr}(\tau)\ d\tau. \qquad (8)$$

The functions G(t) and K(t), or J(t) and B(t) characterize the material and have the names:

J(t) = shear creep compliance.

B(t) = bulk creep compliance.

G(t) = shear relaxation modulus.

K(t) = bulk relaxation modulus.

The material will usually be supposed homogeneous so that all functions are independent of the space coordinates.

The functions are related by Volterra integral equations:

$$\int_o^t G(t-\tau)\, J(\tau)\, d\tau = t, \tag{9}$$

$$\int_o^t K(t-\tau)\, B(\tau)\, d\tau = t. \tag{10}$$

Given $J(t)$, $G(t)$ can be calculated by solving (9) by the method shown in section 2.9; etc.

The uniaxial stress field which is approximated by the tension test is of special importance. If $\sigma_{11} \neq 0$ while the other components of stress are zero, the deviatoric stresses are

$$s_{11} = 2/3\ \sigma_{11},\ s_{22} = -1/3\ \sigma_{11},\ s_{33} = -1/3\ \sigma_{11}, \tag{11}$$

and the others are zero. From equation (4), (7), and (8),

$$\epsilon_{11} = \int_o^t D(t-\tau)\, \dot{\sigma}_{11}\, d\tau\ , \tag{12}$$

$$\epsilon_{22} = \epsilon_{33} = -\int_o^t \nu(t-\tau)\, D(t-\tau)\, \dot{\sigma}_{11}(\tau)\, d\tau. \tag{13}$$

Where,

$$D(t) = 1/3\ J(t) + 1/9\ B(t), \tag{14}$$

$$\nu(t) = \frac{3\ J(t) - 2\ B(t)}{6\ J(t) + 2\ B(t)}\ . \tag{15}$$

The pair of functions $D(t)$ and $\nu(t)$ also characterize the material and have the names:

$D(t)$ - tensile creep compliance,

$\nu(t)$ -"Poisson's Ratio" for creep.

This definition for ν leads to $\epsilon_y = -\nu\, \epsilon_x$ for the uniaxial creep test. This definition is not a unique generalization of the idea of Poisson's ratio for elastic materials.

Solving equations (14) and (15) we have

$$J = 2\,(1+\nu)\,D, \tag{16}$$

$$B = 3\,(1-2\nu)\,D. \tag{17}$$

Thus, the bulk creep compliance and the shear creep compliance and, consequently, the relaxation moduli can all be calculated from the functions $\nu(t)$ and $D(t)$ occurring in the equations describing the tensile test.

The inverse of (12) is

$$\sigma_{11} = \int_o^t E(t-\tau)\, \dot{\epsilon}_{11}(\tau)\, d\tau. \tag{18}$$

The new function is related to the tensile creep compliance by the Volterra integral equation,

$$\int_o^t D(t-\tau)\, E(\tau)\, d\tau = t, \tag{19}$$

and has the name:

$E(t)$ - tensile relaxation modulus.

The complete solution to a problem in linear viscoelasticity is determined by equations (1) - (4)

and a pair of the stress-strain relations such as (5) and (6).

The solution must satisfy certain boundary conditions: Usually the displacement vector is given over part of the boundary while the stress vector F_k is given over the remainder. The stress vector is related to the stress tensor by

$$F_k = \sigma_{km} n_m, \tag{20}$$

where n_m are the components of the unit normal to the surface.

2.2. Elasticity.

The theory of linear elastic materials may be viewed as a special case in the theory of viscoelasticity when

$$J(t) = J_o h(t) \tag{21}$$

and

$$B(t) = B_o h(t), \tag{22}$$

where h(t) is a unit step function:

$$h(t) = \begin{cases} 0, & t < 0 \\ 1, & t > 0 \end{cases}. \tag{23}$$

Then

$$\begin{aligned} G &= G_o\, h(t), \\ K &= K_o\, h(t), \end{aligned} \tag{24}$$

$$D(t) = D_o\, h(t),$$
$$E(t) = E_o\, h(t). \tag{25}$$

The elastic constants G_o, E_o, ν_o, and K_o are related:

$$G_o = \frac{E_o}{2\,(1+\nu_o)}\ , \tag{26}$$

$$K_o = \frac{E_o}{3\,(1-2\nu_o)}\ . \tag{27}$$

The field equations become

$$\partial_m \sigma_{km} + f_k = 0\ , \tag{28}$$

$$\epsilon_{km} = \tfrac{1}{2}\,(\partial_k\, u_m + \partial_m\, u_k), \tag{29}$$

$$s_{km} = \sigma_{km} - 1/3\ \sigma_{rr}\ \delta_{km}, \tag{30}$$

$$e_{km} = \epsilon_{km} - 1/3\ \epsilon_{rr}\ \delta_{km}, \tag{31}$$

$$s_{km} = 2G_o\ e_{km}, \tag{32}$$

$$1/3\ \sigma_{rr} = K_o\ \epsilon_{rr}. \tag{33}$$

Thus, time plays the role of a parameter and does not appear explicitly in the field equations.

2.3. Proportional Loading.

An important class of problems are those for which the stress vector on the surface has the form

$$F_k = \bar{F}_k \, f(t) \tag{34}$$

The superposed bar will denote a function of the space coordinates only. This is termed proportional loading. Let us determine under what conditions the stress field has the form

$$\sigma_{km} = \bar{\sigma}_{km} \, f(t), \tag{35}$$

where $\bar{\sigma}_{km}$ can be determined from the theory of elasticity.

The boundary conditions (20) give

$$\bar{\sigma}_{km} n_m = \bar{F}_k \, . \tag{36}$$

In the absence of body force, the equilibrium equations (1) give

$$\partial_m \bar{\sigma}_{km} = 0 \, . \tag{37}$$

The deviatoric stresses are

$$s_{km} = \bar{s}_{km} \, f(t), \tag{38}$$

where

$$\bar{s}_{km} = \bar{\sigma}_{km} - 1/3 \, \bar{\sigma}_{rr} \, \delta_{km} \, . \tag{39}$$

The stress-strain relations (7) and (8) give

$$e_{km} = \bar{e}_{km} \, g(t) \, , \tag{40}$$

$$\epsilon_{rr} = \bar{\epsilon}_{rr}\, k(t) \ ;$$

where

$$2\,\bar{e}_{km} = 1/G_o\ \bar{s}_{km} \ , \tag{41}$$

$$\bar{\epsilon}_{rr} = 1/3K_o\ \bar{\sigma}_{rr} \ , \tag{42}$$

$$g(t) = G_o \int_o^t J(t-\tau)\ \dot{f}(\tau)\ d\tau \ , \tag{43}$$

$$k(t) = K_o \int_o^t B(t-\tau)\ \dot{f}(\tau)\ d\tau \ . \tag{44}$$

The constants G_o and K_o are arbitrary constants.

Let

$$\bar{\epsilon}_{km} = \bar{e}_{km} + 1/3\ \delta_{km}\ \bar{\epsilon}_{rr}.$$

Then

$$\bar{\epsilon}_{km} = 1/2\ (\partial_k\ \bar{u}_m + \partial_m\ \bar{u}_k) \ , \tag{45}$$

$$u_k = \bar{u}_k\ g(t) \ , \tag{46}$$

only if $g(t) = k(t)$ or $\epsilon_{rr} = 0$; that is, only when $B(t)$ is proportional to $J(t)$ by a constant factor.

From equations (16) and (17),

$$B(t) = 3/2\ \frac{1-2\ \nu(t)}{1+\nu(t)}\ J(t). \tag{47}$$

Thus $B(t)$ is proportional to $J(t)$ only when ν is constant. Further, $\epsilon_{rr} = 0$ only when ν is a constant equal to $1/2$.

If ν is constant, then the stress and displacement are determined by (35) and (46) where the barred quantities satisfy the equations of elasticity, provided the boundary conditions of the viscoelastic

problem agrees with (34), and (46).

In fact ν is never constant for any material. But it frequently happens that the variation in ν with time is slight or the effect of changes in ν on the solution to the elasticity problem is slight. In these cases the stress field under proportional loading can be approximated by the elasticity solution.

2.4. Plane Stress.

If the stress components $\sigma_{k3} = 0$, the equations of viscoelasticity can be simplified to the following:

$$\partial_\beta \sigma_{\alpha\beta} = 0 , \tag{48}$$

$$\epsilon_{\alpha\beta} = 1/2 \, (\partial_\alpha \mu_\beta + \partial_\beta \mu_\alpha) , \tag{49}$$

$$s_{\alpha\beta} = \sigma_{\alpha\beta} - 1/3 \, \sigma_{rr} \, \delta_{\alpha\beta} , \tag{50}$$

$$e_{\alpha\beta} = \epsilon_{\alpha\beta} - 1/3 \, \epsilon_{rr} \, \delta_{\alpha\beta} , \tag{51}$$

$$2e_{\alpha\beta} = \int_o^t J(t-\tau) \, \dot{s}_{\alpha\beta}(\tau) \, d\tau , \tag{52}$$

$$\epsilon_{rr} = \int_o^t 1/3 \, B(t-\tau) \, \dot{\sigma}_{\alpha\alpha}(\tau) d\tau . \tag{53}$$

The Greek indices have the range 1, 2 and all quantities are functions of x^α and t.

The equations (48) - (53) define a plane stress problem. There is an important class of plane stress problems, for which the solution is independent of the material properties, which we now consider. In this

case, the stress can be calculated from the corresponding elasticity solution.

Equations (48) are satisfied by introducing the Airy stress function F:

$$\sigma_{\alpha\beta} = \varepsilon_{\alpha\gamma}\ \varepsilon_{\beta\delta}\ \partial_\gamma\ \partial_\delta\ F. \tag{54}$$

Where $\varepsilon_{\alpha\beta}$ is the permutation symbol ($\varepsilon_{12} = -\ \varepsilon_{21} = 1$, $\varepsilon_{11} = \varepsilon_{22} = 0$).

Eliminating the displacements from (49) gives

$$\varepsilon_{\alpha\delta}\ \varepsilon_{\beta\tau}\ \partial_\tau\ \partial_\delta\ \epsilon_{\alpha\beta} = 0\ . \tag{55}$$

This is the compatibility relation.

Substituting (54) into (50) - (53) and the result into (55) leads to

$$\nabla^4\ F = \partial_\alpha \partial_\alpha \partial_\beta \partial_\beta\ F = 0. \tag{56}$$

If the boundary conditions are solely on stress, the equations (56) and the stress boundary conditions completely determine the stress independent of the material properties and the stress is the same as for an elastic material.

2.5. Short Time Solution.

This section deals with a suddenly applied load and the solution immediately after loading (that is, immediately after all wave propagation effects are completed).

The stress and strain fields are related by (5) and (6). For a step change at time zero,

$$s_{km} = 2G(0)\, e_{km} , \tag{57}$$

$$1/3\ \sigma_{rr} = K(0)\ \epsilon_{rr} . \tag{58}$$

Thus, constitutive relations are identical to the elasticity equations with elastic moduli equal to the values of the relaxation modulus at time zero. Therefore, the stress distribution at the instant of loading will be the same as given by the elasticity solution for shear modulus $G = G(0)$ and bulk modulus $K = K(0)$ or Poisson ratio $\nu = \nu(0)$.

2.6. Long Time Solution.

The viscoelastic materials have a fading memory. That is, the stress due to a step change in strain decreases in time. The result is that when loads are maintained at a constant value, an equilibrium state is reached such that no further change in stress or strain occurs.

By (5) and (6),

$$s_{km}(\infty) = G(\infty)\, e_{km}(\infty) , \tag{59}$$

$$1/3\ \sigma_{rr}(\infty) = K(\infty)\ \epsilon_{rr}(\infty). \tag{60}$$

The constitutive equations again coincide with linear elasticity. In this case the moduli are equal to the

values of the relaxation functions at time infinity. Consequently, if the surface loads remain constant, the stress state will eventually approach that of the elasticity solution for shear modulus $G = G(\infty)$ and Poisson ratio $\nu = \nu(\infty)$.

2.7. Temperature Effects.

Each of the material property functions is temperature dependent. That is, if the tensile test is conducted at different temperatures, the tensile creep compliance is a different function of time. In many instances this temperature dependence can be described by an empirical relation involving the so-called "time-temperature equivalence". The material is then termed thermo-rheologically simple.

Let $G(t)$ be the relaxation modulus at constant temperature T and $\bar{G}(t)$ be the relaxation modulus at some reference temperature T_o:

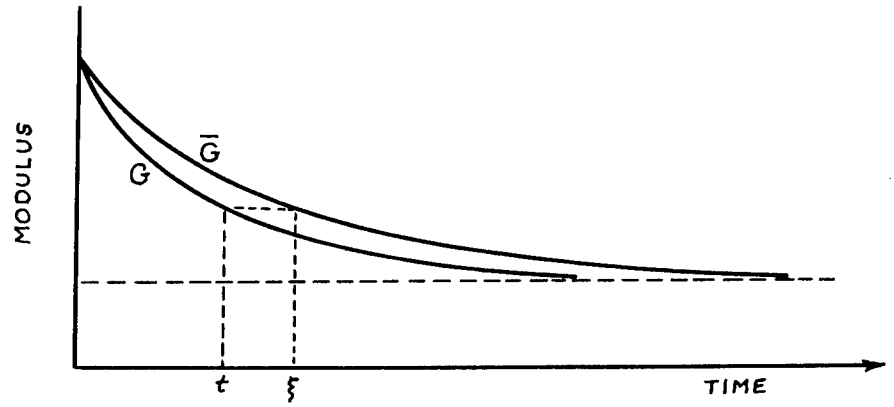

Suppose that the effect of temperature on the short time modulus and long time modulus is such that:

$$G(0) = \overline{G}(0), \tag{61}$$

$$G(\infty) = \overline{G}(\infty). \tag{62}$$

In this case, there always exists a pair of times for which G and $\overline{G}$ have the same value

$$G(t) = \overline{G}(\xi). \tag{63}$$

The time ξ is called the reduced time. It depends on the temperature T of the test and the time t at which the ordinate G is measured.

Empirical evidence suggest that, for isothermal deformation of many materials,

$$\xi = a(T)\, t. \tag{64}$$

The function a(T) of temperature is known as a temperature shift factor (in the sense of shifting the curves, if the figure were plotted on log time).

Similar equations may be found to describe the isothermal values of the other material property functions, but the shift factor is usually different.

Isothermal experiments cannot determine the nature of the stress-strain relationship for tests in which the temperature varies with time and no experimental evidence is available. A possible generalization which

is compatible with the isothermal observations was proposed by Morland and Lee.* Their idea is that rate of change of the modulus is determined by the instantaneous temperature.

If G(t) is the relaxation modulus measured at varying temperature T(t), then (63) holds. Thus

$$\frac{dG}{dt} = \frac{d\bar{G}}{d\xi}\,\frac{d\xi}{dt} \quad . \tag{65}$$

The fundamental hypothesis is that, for varying temperature,

$$\frac{d\xi}{dt} = a(T) \quad . \tag{66}$$

This agrees with (64) in the isothermal case. If temperature is a function of time for a given particle, and the material is homogeneous,

$$\xi(t) = \int_0^t a(T(t))\, dt \quad . \tag{67}$$

This generalizes (64) to the case of varying temperature.

Now suppose the same temperature variation occurs but the strain is applied at time τ. Let $F_\tau(t)$ be the resulting relaxation modulus. Again assuming that the initial and final values are independent of temperature, there exists a function $\xi_\tau(t)$ such that

$$F_\tau(t) = \bar{G}(\xi_\tau) \quad , \tag{68}$$

* Trans. Soc. Rheology, 4, 233-263, (1960).

and

$$\frac{dF_\tau}{dt} = \frac{d\bar{G}}{d\xi_\tau} \frac{d\xi_\tau}{dt} .$$

The fundamental hypothesis is

$$\frac{d\xi_\tau}{dt} = a(T) . \tag{69}$$

Since

$$F_\tau(\tau) = \bar{G}(0) , \tag{70}$$

$$\xi_\tau(\tau) = 0 . \tag{71}$$

Thus,

$$\xi_\tau = \int_0^t a(T(t))\, dt = \xi(t) - \xi(\tau) .$$

The stress due to continuously changing strain is then

$$s_{ij} = \int_0^t 2\, \bar{G}(\xi(t) - \xi(\tau))\, \dot{e}_{ij}(\tau)\, d\tau . \tag{72}$$

This relation is a hypothesis not yet conformed by experiment and it can be expected to give, at best, only approximate representation of the effects of temperature.

2.8. Volterra Integral Equations.

The various functions of time which describe the physical properties of a viscoelastic material are related by integral equations of the form:

$$\int_0^t D(t-\tau)\, E(\tau)\, d\tau = t \ . \qquad (73)$$

The functions D(t) and E(t) have the general form:

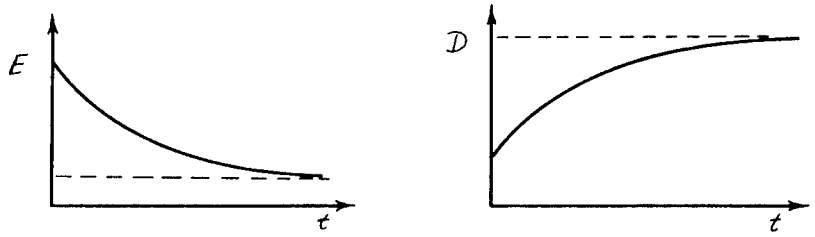

The function E(t) decreases monotonically toward a constant value, while the function D(t) increases monotonically to a constant value. The limiting values are related:

$$E(0) = \frac{1}{D(0)} \ , \qquad (74)$$

and

$$E(\infty) = \frac{1}{D(\infty)} \ . \qquad (75)$$

A fundamental problem of viscoelasticity is to determine one function when the other is known.

Equation (73) has been exhaustively studied and various numerical procedures are known which will, in principle, allow the solution to be approximated as closely as desired. One may, for example, divide the time axis into finite intervals and make use of direct approximation of the integral by some numerical means such as the trapezoidal rule.

In principle, numerical integration leads to the exact answer as the size of the intervals tends to zero. Unfortunately, the various possible numerical procedures that may be used to approximate the integral are very sensitive to errors in the values of the functions and such errors are always introduced by round-off of the numbers. Moreover, the known function is frequently determined by experiment and, owing to experimental error, may not be such a smooth function as the exact value. Any such irregularities tend to magnify enormously if the numerical procedure is not chosen carefully.

Several numerical procedures have been tried in order to determine E(t) when D(t) was known from experiments. The procedure of Hopkins and Hamming* seems to be the best.

---

* J. Appl. Phys., 28, 906-909, (1957).

3. TRANSMISSION OF LIGHT.

3.1. Plane Waves.

Consider a phenomenon which varies with distance z and time t according to the law

$$a \cos (kz - \omega t + \epsilon), \tag{1}$$

where a, k, ω, ϵ are constants. Such a phenomenon is referred to as a wave. The factor "a" is the amplitude and the argument of the cosine function is the phase.

When considering the solution to a differential equation for a real variable, it is often convenient to consider the variable to be a complex number. The real and imaginary parts of the complex variable are then each solutions of the differential equation for the real variable.

The function (1) is the real part of the complex variable

$$\alpha e^{i\varphi}, \tag{2}$$

where α is a complex number and

$$\varphi = kz - \omega t . \tag{3}$$

Any phenomenon represented by (2) is also called a wave.

This representation of a wave by complex variables can be extended to vector valued functions: A complex vector will mean an entity for which the real

and imaginary parts are real vectors. Vectors will be denoted by a subposed tilde. A vector valued wave then has the form

$$\underset{\sim}{a}\, e^{i\varphi}\,, \qquad (4)$$

$$\varphi = k\, \underset{\sim}{n} \cdot \underset{\sim}{r} - \omega t.$$

The complex constant vector $\underset{\sim}{a}$ will be called the amplitude vector. The real unit vector $\underset{\sim}{n}$ defines the direction of propagation. The real vector $\underset{\sim}{r}$ is the position vector. The frequency of the wave is ω. The wave number is k. The wave speed is defined as

$$v = \frac{\omega}{k}\,.$$

The wave length is defined as

$$\lambda = \frac{2\pi}{k}\,.$$

Let the real part of a complex quantity be denoted by a superscript +, the imaginary part by a superscript -, and the conjugate by a superscript *. The following terminology is used.

$\underset{\sim}{a} \cdot \underset{\sim}{a} = 0$ - circularly polarized,

$\underset{\sim}{a}^{*} \times \underset{\sim}{a} = 0$ - linearly polarized,

$\underset{\sim}{a} \cdot \underset{\sim}{n} = 0$ - transverse.

If $\underset{\sim}{a}^{+}$, $\underset{\sim}{a}^{-}$, and $\underset{\sim}{n}$ form a right-handed system, the wave is called right-handed. Only right-handed transverse waves are considered in the following.

The real part of the complex wave is given by

$$R(\underset{\sim}{E}) = \underset{\sim}{a}^{+} \cos \varphi - \underset{\sim}{a}^{-} \sin \varphi \quad .$$

Let $\underset{\sim}{g}_i$ be the base vectors and

$$\underset{\sim}{a}^{+} = a_i^{+} \underset{\sim}{g}_i \ , \ \underset{\sim}{a}^{-} = a_i^{-} \underset{\sim}{g}_i \ .$$

Then

$$\begin{aligned} R(\underset{\sim}{E}) = \ & Q_1 \cos(\varphi + \epsilon_1) \underset{\sim}{g}_1 \\ & + Q_2 \cos(\varphi + \epsilon_2) \underset{\sim}{g}_2 \\ & + Q_3 \cos(\varphi + \epsilon_3) \underset{\sim}{g}_3 \ , \end{aligned} \tag{5}$$

where

$$Q_i = \sqrt{\left(a_i^{+}\right)^2 + \left(a_i^{-}\right)^2}$$

and

$$\tan \epsilon_i = \frac{a_i^{-}}{a_i^{+}} \qquad \text{(no sum)} \ .$$

Thus the vector valued wave may be regarded as three waves; each has the same frequency and wave number but different amplitudes and different phases.

The case of a transverse wave propagating along the z-axis will be of particular interest. Then $\underset{\sim}{a}^{+}$ and $\underset{\sim}{a}^{-}$ lie in the x-y plane and $Q_3 = 0$. The vector expression (5) represents two waves of different amplitude and phase.

For the linearly polarized wave, $\underset{\sim}{a}^{*} \times \underset{\sim}{a} = 0$. This implies that $\underset{\sim}{a}^{+} \times \underset{\sim}{a}^{-} = 0$. Thus, $\underset{\sim}{a}^{+}$ and $\underset{\sim}{a}^{-}$ are parallel. In that case, $\epsilon_1 = \epsilon_2$; the phase is the same but the

amplitude may be different:

$$R(\underset{\sim}{E}) = Q_1 \cos(\varphi + \epsilon)\, \underset{\sim}{g}_1 + Q_2 \cos(\varphi + \epsilon)\, \underset{\sim}{g}_2 . \quad (6)$$

For a circularly-polarized transverse wave propagated along the z-axis, the requirement $\underset{\sim}{a} \cdot \underset{\sim}{a} = o$ implies the $\underset{\sim}{a}^{+} \cdot \underset{\sim}{a}^{-}$ are orthogonal and have the same length. In this case, the amplitudes are the same and the phase of the two component waves differ by $\pi/2$:

$$R(\underset{\sim}{E}) = Q \cos(\varphi + \epsilon)\, \underset{\sim}{g}_1 + Q \sin(\varphi + \epsilon - \tfrac{\pi}{2})\, \underset{\sim}{g}_2 . \quad (7)$$

3.2. Dielectrics.

This section is devoted to the theory of birefringence based upon the description of light as an electromagnetic wave propagating in an anisotropic dielectric. The applications will be limited to quasi-static deformations so that, during the time of passage of an electromagnetic wave, the displacements of the material are negligible. The equations of a dielectric at rest can therefore be used. Furthermore, since only the relative intensity of monochromatic light will be observed, the absorption and dispersion will be neglected.

The equations of an anisotropic dielectric then have the following form:

$$\text{curl } \underset{\sim}{H} - \frac{\partial \underset{\sim}{D}}{\partial t} = 0 \ . \tag{8}$$

$$\text{curl } \underset{\sim}{E} + \frac{\partial \underset{\sim}{B}}{\partial t} = 0 \ . \tag{9}$$

$$D_i = \epsilon_o K_{ij} E_j \ . \tag{10}$$

$$\underset{\sim}{H} = \frac{1}{\mu_o} \underset{\sim}{B} \ . \tag{11}$$

The fields $\underset{\sim}{D}$ and $\underset{\sim}{B}$ are also subject to the relations

$$\text{div } \underset{\sim}{B} = 0 \ ,$$

$$\text{div } \underset{\sim}{D} = 0 \ ;$$

but these will be satisfied trivially by the solution which will be obtained for (8) - (11).

The tensor K_{ij} will be called the dielectric tensor. It is regarded in this chapter as known and constant. The term "anisotropic", as used here, merely means that the dielectric tensor does not reduce to a scalar multiple of the unit matrix. The ϵ_o and μ_o are fundamental electromagnetic constants.

At a surface with unit normal vector $\underset{\sim}{\nu}$, the fields are subject to the jump conditions:

$$\underset{\sim}{\nu} \times [\underset{\sim}{E}] = 0 \ , \qquad \underset{\sim}{\nu} \times [\underset{\sim}{H}] = 0 \ , \tag{12}$$

$$\underset{\sim}{\nu} \cdot [\underset{\sim}{D}] = 0 \ , \qquad \underset{\sim}{\nu} \cdot [\underset{\sim}{B}] = 0 \ . \tag{13}$$

It will turn out for the problems considered that the relations (13) are identically satisfied when the relations (12) are satisfied and consequently they are

not used here.

Consider a plane wave , propagating in the material, given by the fields:

$$\begin{aligned} \underset{\sim}{E} &= \underset{\sim}{a}\, e^{i\omega} \quad , \\ \underset{\sim}{B} &= \underset{\sim}{b}\, e^{i\omega} \quad , \\ \underset{\sim}{D} &= \underset{\sim}{d}\, e^{i\omega} \quad , \\ \underset{\sim}{H} &= \underset{\sim}{h}\, e^{i\omega} \quad , \\ \omega &= k\, \underset{\sim}{n}\cdot\underset{\sim}{r} - \omega t \quad , \end{aligned} \tag{14}$$

where $\underset{\sim}{a}$, $\underset{\sim}{b}$, $\underset{\sim}{d}$, $\underset{\sim}{h}$ are constant complex amplitude vectors.

The field equations (8) - (11) give

$$\underset{\sim}{b} = \frac{k}{\omega}\, \underset{\sim}{n} \times \underset{\sim}{a} \quad , \tag{15}$$

$$\underset{\sim}{d} = -\frac{k}{\omega}\, \underset{\sim}{n} \times \underset{\sim}{h} \quad , \tag{16}$$

$$\underset{\sim}{h} = \frac{1}{\mu_o}\, \underset{\sim}{b} \quad , \tag{17}$$

$$a_i = \frac{1}{\epsilon_o}\, K^{-1}_{ij}\, d_j \quad . \tag{18}$$

Therefore the real parts of the vectors have the relation:

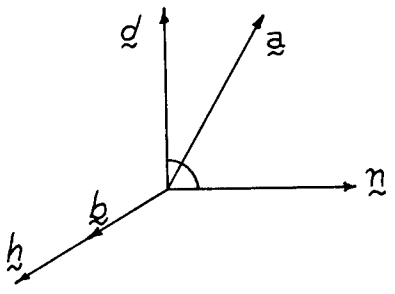

The index of refraction N is defined by

$$N = \frac{kc}{\omega} \quad , \tag{19}$$

where

$$c = \frac{1}{\sqrt{\mu_o \, \epsilon_o}} \quad . \tag{20}$$

Eliminating $\underset{\sim}{b}$ and $\underset{\sim}{d}$ gives the equations:

$$a_i = - \mu_o c \, N \, K^{-1}_{ij} \, e_{jrs} \, n_r \, h_s \quad , \tag{21}$$

$$(\delta^j_i - N^2 \, \delta^{jrm}_{ipq} \, K^{-1}_{qm} \, n_p \, n_r) \, h_j = 0 \quad . \tag{22}$$

The relation (22) represents three homogeneous equations for the components of the real or the imaginary parts of $\underset{\sim}{h}$. Thus, a wave exists only when the determinant of the coefficients is zero:

$$\det = 1 - N^2 \, \delta^{st}_{ab} \, n_a \, n_t \, K^{-1}_{bs} + \tag{23}$$

$$+ N^{4\frac{1}{2}} \, (\delta^{st}_{ba} \, \delta^{ik}_{me} - \delta^{ik}_{ba} \, \delta^{st}_{me}) n_a \, n_t \, n_k \, n_e \, K^{-1}_{bs} K^{-1}_{mi} = o$$

The δ- symbols are the generalized Kronicker delta.

Since $N > o$, there are exactly two indices of refraction, N_1 and N_2, determined by the roots to (23). If K_{ij} is symmetric and $N_1 \neq N_2$, the two corresponding solutions of (22) are orthogonal vectors. Consider the coordinate system with the z axis along $\underset{\sim}{n}$ and the x, y axes along the directions determined by the solutions

of (22). In this particular coordinate system,

$$K_{12} = K_{21} = 0 \ .$$

That is, the two possible directions of $\underset{\sim}{h}$ are the secondary principal axis of K_{ij} in the plane normal to $\underset{\sim}{n}$. The solution with $\underset{\sim}{h}$ along the y-axis gives

$$\begin{aligned} N &= N_1 = \sqrt{K_{11}} \ , \\ a_1 &= \frac{1}{N_1} \mu_o \, c \, h_2 \ , \\ a_2 &= 0 \ , \\ a_3 &= N_1 \, K_{31}^{-1} \mu_o \, c \, h_2 \ . \end{aligned} \tag{24}$$

The solution with $\underset{\sim}{h}$ along the x-axis is

$$\begin{aligned} N &= N_2 = \sqrt{K_{22}} \ , \\ a_1 &= 0 \ , \\ a_2 &= \frac{-1}{N_2} \mu_o \, c \, h_1 \ , \\ a_3 &= -N_2 \, K_{32}^{-1} \mu_o \, c \, h_1 \ . \end{aligned} \tag{25}$$

Thus, the two indices of refraction are the secondary principal values of K_{ij} in the plane normal to $\underset{\sim}{n}$.

The case where $\underset{\sim}{n}$ is normal to one of the principal axes is of particular interest. It is then most convenient to take the coordinate axes along the principal directions of K_{ij}. Consider the case when $\underset{\sim}{n}$ is normal to the y-axis. For one of the two waves,

$\underset{\sim}{h}$ is along the y-axis:

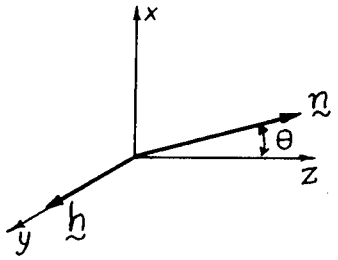

In this case,

$$N = N_1 = \sqrt{\frac{1}{K_1^{-1}\cos^2\theta + K_3^{-1}\sin^2\theta}} \quad ,$$

$$a_1 = N_1 \mu_o c K_1^{-1} \cos\theta \, h_2 \quad , \tag{26}$$

$$a_2 = 0 \quad ,$$

$$a_3 = - N_1 \mu_o c K_3^{-1} \sin\theta \, h_1 \quad .$$

For the second wave, the vector $\underset{\sim}{a}$ is along the y-axis, and $\underset{\sim}{h}$ is normal to $\underset{\sim}{n}$ and $\underset{\sim}{a}$.

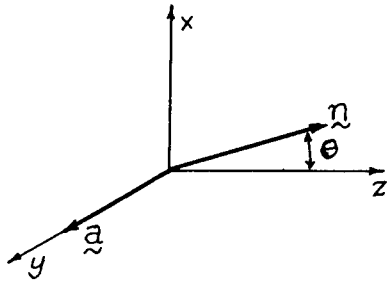

In this case,

$$N = N_2 = \sqrt{K_2} \quad ,$$

$$\underset{\sim}{h} = N_2 \varepsilon_o c \, \underset{\sim}{n} \times \underset{\sim}{a} \quad . \tag{27}$$

The K_1, K_2, K_3 are the principal values of the tensor K_{ij}. Similar results hold when $\underset{\sim}{n}$ is normal to the first principal direction.

In every case the real and imaginary parts of each field are determined by the same relations. They are therefore parallel and each field is a linearly polarized wave in the sense of section 3.1. The field $\underset{\sim}{H}$ is also a transverse wave.

The direction of $\underset{\sim}{a}$ is called the direction of vibration. The direction of $\underset{\sim}{h}$ is called the direction of polarization. It will be most convenient in the following sections to select the vector $\underset{\sim}{h}$ as fundamental. The vector $\underset{\sim}{a}$ is then determined by one of the relations (24) - (27).

3.3. Normal Incidence.

The solution of equations (8) to (11) subject to appropriate boundary conditions gives the laws of the reflection and refraction of light. These results are usually given in the form of geometric constructions which are very tedious to follow or else in approximate forms for which the nature of the approximation is not clear. The following sections give an analytical expression to the optical laws which will be needed in photomechanics.

Consider a slice of the dielectric which is assumed to be homogeneous, i.e., K_{ij} is constant. Choose the coordinate axes so that the surfaces of the slice are $z = 0$ and $z = h$.

If a plane, transverse wave is incident normal to one of the surfaces, part of the wave is reflected and part is transmitted. A similar reflection and transmission occurs at the second surface. There are, therefore, five electromagnetic waves having the following directions:

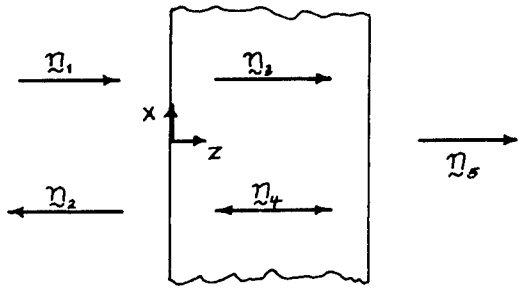

A solution to the field equations is required when the incident wave is a plane transverse wave

$$\underset{\sim}{H}_1 = \underset{\sim}{h}_1 e^{i\varphi_1}, \quad \varphi_1 = k_o \underset{\sim}{n}_1 \cdot \underset{\sim}{r} - \omega t.$$

If $\underset{\sim}{h}_1$ is parallel to one of the secondary principal directions of K_{ij} in the plane z = constant, the fields

$$\underset{\sim}{H}_2 = \underset{\sim}{h}_2 e^{i\varphi_2}, \quad \varphi_2 = k_o \underset{\sim}{n}_2 \cdot \underset{\sim}{r} - \omega t,$$

$$\underset{\sim}{H}_3 = \underset{\sim}{h}_3 e^{i\varphi_3}, \quad \varphi_3 = k \underset{\sim}{n}_3 \cdot \underset{\sim}{r} - \omega t,$$

$$\underset{\sim}{H}_4 = \underset{\sim}{h}_4 \, e^{i\varphi_4} \, , \quad \varphi_4 = k \, \underset{\sim}{n}_4 \cdot \underset{\sim}{r} - \omega t \, ,$$

$$\underset{\sim}{H}_5 = \underset{\sim}{h}_5 \, e^{i\varphi_5} \, , \quad \varphi_5 = k_o \underset{\sim}{n}_5 \cdot \underset{\sim}{r} - \omega t \, ,$$

have $\underset{\sim}{h}_2$, $\underset{\sim}{h}_3$, $\underset{\sim}{h}_4$, and $\underset{\sim}{h}_5$ parallel to that principal direction.

There are two fundamental cases, according to whether $\underset{\sim}{h}$ is parallel to one or the other principal directions. The internal fields in each case are determined by (24) or (25). The solution for an arbitrary wave is a linear combination of these two cases.

In each case, the jump conditions (12), applied at each face, lead to the solution

$$\underset{\sim}{H}_5 = C \, e^{i(\theta - k_o h)} \, \underset{\sim}{H}_1 \tag{28}$$

and

$$\underset{\sim}{E}_5 = C \, e^{i(\theta - k_o h)} \, \underset{\sim}{E}_1 \, , \tag{29}$$

where

$$C = \frac{2N}{\sqrt{4N^2 \cos^2 kh + (1+N^2)^2 \sin^2 kh}} \, , \tag{30}$$

$$\tan \theta = \frac{1+N^2}{2N} \tan kh \, , \tag{31}$$

and N is given by (24) or (25).

CR-444

3.4. Oblique Incidence.

Consider the case when the normal to the surface of the slice of dielectric is a principal axes of K_{ij}. Choose the coordinates along the principal axes of K_{ij}. The instance when the wave propagated in the dielectric is perpendicular to the y-axis will now be considered.

The secondary principal axes of K_{ij} then coincide with the y-axis and the normal to the y-axis. The two waves given by (26) and (27) are then possible.

Consider first the case when the incident wave has $\underset{\sim}{h}$ parallel to the y-axis. The reflected and transmitted waves turn out to all have $\underset{\sim}{h}$ parallel to the y-axis. The five fields have the directions shown:

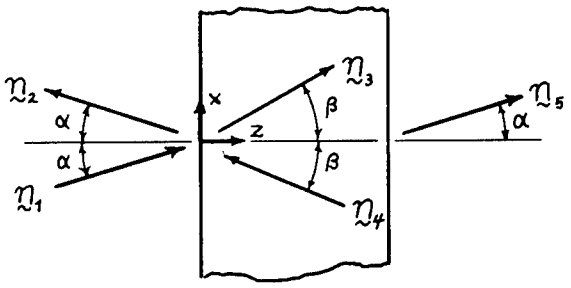

Applying the jump conditions (12) to these waves and using the solution (26) leads to the relation between incident and transmitted waves:

$$\underset{\sim}{H}_5 = C\, e^{i(\theta - k_o h \cos \alpha)}\, \underset{\sim}{H}_1 \qquad (32)$$

and

$$\underset{\sim}{E}_5 = C\, e^{i(\theta - k_o h \cos\alpha)}\ \underset{\sim}{E}_1 \ , \tag{33}$$

where

$$C = \frac{2f}{\sqrt{4f^2\cos^2\gamma + (1+f^2)^2\sin^2\gamma}} , \tag{34}$$

$$\tan\theta = \frac{1+f^2}{2f}\tan\gamma \ , \tag{35}$$

$$\gamma = kh\cos\theta \ , \tag{36}$$

$$f = \frac{N\cos\theta}{K_1\cos\alpha} \ , \tag{37}$$

$$\sin\theta = \frac{1}{N}\sin\alpha \ , \tag{38}$$

$$N = N_1 = \frac{1}{\sqrt{K_1^{-1}\cos^2\theta + K_3^{-1}\sin^2\beta}} \ , \tag{39}$$

and K_1, K_2, K_3, are the principal values of K_{ij}.

Consider next the case when the incident wave has $\underset{\sim}{h}$ normal to the y-axis. Then the solution (27) appliés. Using the jump conditions, the relation between incident and transmitted waves is again found to have the form given above but with f and N given by new formulae:

$$f = \frac{N\cos\theta}{\cos\alpha} \ , \tag{40}$$

$$N = N_2 = \sqrt{K_2} \ . \tag{41}$$

Every incident wave normal to the y-axis can be represented as a linear combination of these two cases.

Similar results hold when the incident wave is normal to the x-axis.

When the wave is along the z-axis, the results coincide with equation (30) and (31).

3.5. Slightly anisotropic, transparent materials.

The materials used in photomechanics are transparent isotropic materials for which straining causes a small change in dielectric properties. Let N_o denote the index of refraction in the undisturbed state and consider the propagation of light through a slice of thickness h. The dielectric tensor can be written

$$K_{ij} = N_o^2 \left(\delta_{ij} + \frac{c}{\omega h} P_{ij}\right) , \qquad (42)$$

where P_{ij} depends on the strain history and is zero in the undisturbed state.

The exact relations of sections 3.3. and 3.4. for propagation of light through a slice will now be investigated for the case when

a) the material is slightly anisotropic, i.e., when P_{ij} is of order unity, and

b) the material is nearly transparent, i.e., when N_o is of order unity.

There are two kinds of approximation involved. The first is that the second term in (1) is small because

$$\epsilon = \frac{c}{\omega h} \ll 1 \ . \tag{43}$$

The parameter ϵ is a non-dimensional characteristic number of the problem, usually having a magnitude about 10^{-5}. Therefore terms of higher order in ϵ can be neglected. The second is that the components K_{ij} are of order unity. In fact N_o is about 1.5, but the error involved by the second approximation does not exceed a few per cent, especially when only relative retardation is observed.

Consider first the results for normal incidence. The index of refraction is given by (24) or (25). Thus,

$$N_1 = \sqrt{N_o^2 \ (1 + \epsilon \ P_{11})} \doteq N_o(1 + \tfrac{1}{2} \epsilon \ P_{11}), \tag{44}$$

$$N_2 = \sqrt{N_o^2 \ (1 + \epsilon \ P_{22})} \doteq N_o(1 + \tfrac{1}{2} \epsilon \ P_{22}). \tag{45}$$

Equations (44) and (45) are of the form

$$N \doteq N_o + \epsilon\delta \ . \tag{46}$$

Thus

$$kh = \frac{N}{\epsilon} \doteq N_o \frac{1}{\epsilon} + \delta \ . \tag{47}$$

For simplicity, suppose that ϵ is chosen such that the large number $N_o \frac{1}{o\epsilon}$ is an integer multiple of 2π. Then

$$\sin kh = \sin \left(N_o \frac{1}{o\epsilon} + \delta\right) = \sin \delta \ , \tag{48}$$

$$\cos kh = \cos \left(N_o \frac{1}{o\epsilon} + \delta\right) = \cos \delta \ . \tag{49}$$

The relation (31) becomes

$$\tan \theta \doteq \frac{1+N_o^2}{2N_o} \tan \delta \ , \tag{50}$$

for slightly birefringent materials.

If N_o is 1.5, $\frac{1+N_o^2}{2N_o} = 1.08$.

As N_o approaches unity, this factor approaches unity. Thus, in the two cases (44) and (45),

$$\theta_1 \doteq \tfrac{1}{2} N_o P_{11} \tag{51}$$

and

$$\theta_2 \doteq \tfrac{1}{2} N_o P_{22} \ , \tag{52}$$

for nearly transparent materials.

The relation (30) becomes

$$C \doteq \frac{2N_o}{\sqrt{4 N_o^2 \cos^2\theta + (1+N_o^2)\sin^2\theta}} \ , \tag{53}$$

for slightly birefringent materials.

The absolute value of C has the bounds

$$\frac{2N_o}{1+N_o^2} < C < 1.$$

The value is therefore nearly unity for nearly transparent materials:

$$C \doteq 1 . \tag{54}$$

Secondly, consider the problem of oblique incidence solved in section 3.4. From (42),

$$K_1 = N_o^2 (1 + \epsilon P_1) . \tag{55}$$

Thus,

$$K_1^{-1} \doteq N_o^{-2} (1 - \epsilon P_1) . \tag{56}$$

Similar expressions hold for K_2 and K_3 .

The relations (37) to (39) lead to

$$\sin \beta \doteq \frac{1}{N_o} \sin \alpha,$$

$$f \doteq \frac{\cos \beta}{N_o \cos \alpha} , \tag{57}$$

$$N_1 \doteq N_o (1 + \tfrac{1}{2} P_1 + \tfrac{1}{2} P_3 \tan^2 \beta) .$$

Thus,

$$\gamma \doteq \frac{N_o \cos \beta}{\epsilon} + \delta ,$$

where

$$\delta = \tfrac{1}{2} N_o \cos \beta \, (P_1 + P_3 \tan^2 \beta) \, . \qquad (58)$$

Choosing ϵ so that $(N_o \cos \beta)/\epsilon$ is a multiple of 2π, (35) becomes

$$\tan \theta = \frac{1+f^2}{2f} \tan \delta \, . \qquad (59)$$

If the angle of incidence varies, for example, from zero to 45^o and $N_o = 1.5$,

$$0.667 \leq f \leq 0.833 \, .$$

In this case

$$1.01 \leq \frac{1+f^2}{2f} \leq 1.08.$$

Therefore, only a small error is made, if (59) is replaced by

$$\theta \doteq \delta \qquad (60)$$

and (34) is replaced by

$$C \doteq 1 \, . \qquad (61)$$

If equations (40) and (41) are used, then (60) and (61) again hold but with

$$\delta = \tfrac{1}{2} \frac{P_2}{\cos \beta} \, . \qquad (62)$$

in place of (58).

The two waves transmitted at oblique incidence therefore have, approximately,

$$\theta_1 = \frac{N_o}{2} P_1 \cos \beta + \frac{N_o}{2} \frac{\sin^2 \beta}{\cos \beta} , \tag{63}$$

$$\theta_2 = \frac{N_o}{2} \frac{P_2}{\cos \beta} , \tag{64}$$

when the material is slightly anisotropic and nearly transparent. These equations reduce to (51) and (52) for normal incidence.

3.6. Approximate Optical Relations.

The exact expressions of sections 3.3 and 3.4 for transmission of light through a slice of dielectric are rather complicated because of the losses due to reflection at the entering and exiting surfaces. It was shown in section 3.5 how the formulae for light transmitted through a slice could be approximated when the material is nearly transparent and only slightly anisotropic. The approximate relations are now summarized.

Consider the case of normal incidence when the normal to the surfaces of the slice is a principal axis of the dielectric tensor. Let $\underset{\sim}{p}$ be a unit vector along the first principal axis (with index of refraction N_1 and wave number k_1) and $\underset{\sim}{q}$ be a unit vector along

the second principal axis (with index of refraction N_2 and wave number k_2) of the dielectric tensor. Let the incident wave be

$$\underset{\sim}{H}_I = \underset{\sim}{h}_I \, e^{i\varphi} , \tag{65}$$

$$\underset{\sim}{h}_I = h_1 \underset{\sim}{P} + h_2 \underset{\sim}{q}, \tag{66}$$

where h_1 and h_2 may be complex constants. The transmitted wave is given by (28) applied to each component. Using the approximate expressions (51), (52) and (54), the transmitted wave is

$$\underset{\sim}{H}_T = \underset{\sim}{h}_T \, e^{i\varphi} , \tag{67}$$

$$\underset{\sim}{h}_T = h_1 \underset{\sim}{p} \, e^{i(\theta_1 - k_o h)} + h_2 \underset{\sim}{q} \, e^{i(\theta_2 - k_o h)}, \tag{68}$$

$$\theta_1 = \tfrac{1}{2} N_o \, p_1 , \tag{69}$$

$$\theta_2 = \tfrac{1}{2} N_o \, p_2 . \tag{70}$$

In the case of oblique incidence at angle α but normal to the second principal axis of the dielectric tensor, the transmitted wave given by

$$\underset{\sim}{h}_T = h_1 \underset{\sim}{p} \, e^{i(\theta_1 - k_o h \cos\alpha)} + h_2 \underset{\sim}{q} \, e^{i(\theta_2 - k_o h \cos\alpha)}, \tag{71}$$

$$\theta_1 = \frac{N_o}{2} p_1 \cos^2\beta + \frac{N_o}{2} p_3 \frac{\sin^2\beta}{\cos\beta} , \tag{72}$$

$$\theta_2 = \frac{N_o}{2} \frac{p_2}{\cos\beta} , \tag{73}$$

$$\sin\beta = \frac{1}{N_o} \sin\alpha . \tag{74}$$

The exact expressions for transmission of light may also be approximated by simple relations in the case of certain special materials. Two examples - the polarizer and the quarter-wave plate - are of particular interest.

An ideal quarter-wave plate is a slice of dielectric for which waves with $\underset{\sim}{h}$ along the first principal axis are not retarded while waves with $\underset{\sim}{h}$ along the second principal axis are retarded by ninety degrees. Thus (68) becomes

$$\underset{\sim}{h}_T = h_1 \underset{\sim}{P} + h_2 e^{-i\pi/2} \underset{\sim}{q}. \tag{75}$$

The real part of the incident wave, according to (5) is

$$R(\underset{\sim}{H}_I) = Q_1 \cos(\varphi + \epsilon_1) \underset{\sim}{p} + Q_2 \cos(\varphi + \epsilon_2) \underset{\sim}{q}. \tag{76}$$

The real part of the transmitted wave is

$$R(\underset{\sim}{H}_T) = Q_1 \cos(\varphi + \epsilon_1) \underset{\sim}{p} + Q_2 \cos(\varphi + \epsilon_2 - \pi/2) \underset{\sim}{q}. \tag{77}$$

A situation of particular interest occurs when the incident wave is a plane polarized wave with $\underset{\sim}{h}$ making an angle of 45° from $\underset{\sim}{p}$ toward $\underset{\sim}{q}$. Then $Q_1 = Q_2 = Q$ and $\epsilon_1 = \epsilon_2 = \epsilon$. The transmitted wave is, according to (7), circularly polarized.

An ideal polarizer is a dielectric for which the first principal index of refraction is nearly unity and the second is very large. From (30), it is seen that when $\underset{\sim}{h}$ is parallel to the first principal axis $C \doteq 1$ and when $\underset{\sim}{h}$ is parallel to the second principal axis $C \doteq 0$. Given an incident wave

$$\underset{\sim}{H}_I = \underset{\sim}{h}\, e^{i\varphi} \quad , \tag{78}$$

the transmitted wave is

$$\underset{\sim}{H}_T = (\underset{\sim}{h} \cdot \underset{\sim}{p})\, \underset{\sim}{p}\, e^{i\varphi}. \tag{79}$$

The real part of the incident wave, referred to arbitrary x-y axis in the plane of the slice, is

$$R(\underset{\sim}{H}_I) = Q_1 \cos(\varphi + \epsilon_1)\, \underset{\sim}{g}_1 + Q_2 \cos(\varphi+\epsilon_2)\, \underset{\sim}{g}_2.$$

The real part of the transmitted wave is

$$\begin{aligned} R(\underset{\sim}{H}_T) = {} & Q_1 \cos\alpha \cos(\varphi + \epsilon_1)\, \underset{\sim}{p} \\ & + Q_2 \sin\alpha \cos(\varphi + \epsilon_2)\, \underset{\sim}{p} \end{aligned} \tag{80}$$

when α is the angle between the axis of the polarizer and the x - axis.

3.7. Plane-Polariscope.

The term polariscope is a general expression referring to any of various possible arrangements of polarizer and quarter-wave plates in order to view a

nearly transparent dielectric. In the plane-polariscope, light is passed through a polarizer, and then through a second polarizer (called the analyzer). The transmitted light exhibits interference fringes which are now investigated.

Let the unit vector $\underset{\sim}{p}$ be directed along the axis of the polarizer. Then, by (79), the light from a monochromatic source which is transmitted by the polarizer is such that

$$\underset{\sim}{H} = A\,\underset{\sim}{p}\,e^{i\varphi}. \tag{81}$$

The origin of coordinates can be chosen so that A is a real number.

Choose the z-axis normal to the dielectric and let the x-y axes be directed along the secondary principal axes of the dielectric tensor. Only the case of normal incidence will be considered, but identical results hold for the oblique incidence.

Let ζ be the angle between $\underset{\sim}{p}$ and the x-axis:

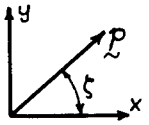

The wave incident on the dielectric is such that

$$\underset{\sim}{H} = (A\cos\zeta\,\underset{\sim}{g}_1)+(A\sin\zeta\,\underset{\sim}{g}_2)\,e^{i\varphi}. \tag{82}$$

By (68), the transmitted light is given by

$$\underset{\sim}{H} = \left\{ A \cos \zeta \; e^{i(\theta_1 - k_o h)} \underset{\sim}{g}_1 + A \sin \zeta \; e^{i(\theta_2 - k_o h)} \underset{\sim}{g}_2 \right\} e^{i\varphi}. \tag{83}$$

The light is next passed through the analyzer. Two cases are of special interest.

Case 1: Crossed Polarizer-Analyzer.

Let the axis of the analyzer be described by the unit vector $\underset{\sim}{q}$. Consider the case when $\underset{\sim}{q}$ makes an angle $\zeta + \pi/2$ with the x-axis:

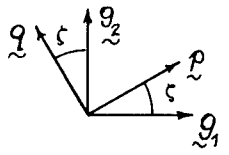

The light transmitted by the analyzer is then, by (79),

$$\underset{\sim}{H} = \left\{ - A \cos \zeta \sin \zeta \; e^{i(\theta_1 - k_o h)} + A \sin \zeta \cos \zeta \; e^{i(\theta_2 - k_o h)} \right\} \underset{\sim}{q} \; e^{i\varphi} = H \underset{\sim}{q}. \tag{84}$$

The real part is

$$R(H) = A \sin 2\zeta \sin n\pi \cos(\varphi - k_o h - \epsilon), \tag{85}$$

where

$$n = \frac{\theta_1 - \theta_2}{2\pi} \tag{86}$$

and ϵ is determined by θ_1 and θ_2. The variable n is called the fringe order.

It can be seen from (85) that there will be zero light intensity at those points for which the principal axes of the dielectric make an angle of zero or 90° with the axis of the polarizer. The locus of all such points form lines on the model called isoclinic lines.

There will also be zero light intensity where the fringe order n is an integer. The locus of all such points form lines on the model which are called isochromatic lines.

If the loss of light by reflection is not neglected, it is found that the isochromatics are only approximately given by integer fringe orders and the intensity is not zero. But, this approximation seems to be adequate for nearly transparent materials.

Case 2: Parallel Polarizer-Analyzer.

Let the axis of the analyzer have the same direction as the polarizer, i.e. $\underset{\sim}{p} = \underset{\sim}{q}$. Then, by (79), the light transmitted by the analyzer is

$$\begin{aligned} \underset{\sim}{H} = & \left\{ A \cos^2\zeta \; e^{i(\theta_1 - k_o h)} \right. \\ & \left. + A \sin^2\zeta \; e^{i(\theta_2 - k_o h)} \right\} e^{i\varphi} \underset{\sim}{p} \qquad (87) \\ = & \; H \underset{\sim}{p} . \end{aligned}$$

The real part is given:

$$R(H) = A\,Q\cos(\varphi - k_o h + \epsilon), \tag{88}$$

where

$$Q^2 = \cos^4\zeta + \sin^4\zeta + 2\cos^2\zeta\sin^2\zeta\cos 2n\pi. \tag{89}$$

The minimum values of Q occur when n is an odd multiple of $\frac{1}{2}$. The isochromatic lines, in this case connect all points for which n is $\frac{1}{2}$, 3/2, etc. They are referred to as half-order fringes.

3.8. Circular-Polariscope.

The isoclinic lines and the isochromatic lines are superposed in the case of the plane polariscope. In order to observe the isochromatic pattern more easily, a circular-polariscope is used. The circular-polariscope consists of polarizer, quarter-wave plate, model, quarter-wave plate, and analyzer. As will now be shown, the isoclinic lines do not appear on the model.

Let $\mathfrak{p}_1$ be the axis of the polarizer. Let $\mathfrak{p}_2$ and $\mathfrak{q}_2$ be the axis of the quarter-wave plate. Only the case when $\mathfrak{p}_1$ makes an angle of 45° between $\mathfrak{p}_2$ and $\mathfrak{q}_2$ will be considered:

The light transmitted by the polarizer and quarter-wave plate combination is, according to section 3.6, circularly polarized:

$$\underset{\sim}{H} = A\ (\underset{\sim}{p}_2 - i\ \underset{\sim}{q}_2)\ e^{i\varphi} = A\ (\underset{\sim}{g}_1 - i\underset{\sim}{g}_2)e^{i(\varphi+\zeta)}. \quad (90)$$

Again A can be chosen to be a real number.

The light is then passed through a nearly transparent dielectric. Let the x-y axis be principal axis of the dielectric. The transmitted wave is given by (68):

$$\underset{\sim}{H} = A\ e^{i(\varphi\ +\ \zeta - k_o h)} \left\{ \underset{\sim}{g}_1\ e^{i\theta_1} - i\ \underset{\sim}{g}_2\ e^{i\theta_2} \right\} \quad (91)$$

$$= A\ e^{i(\varphi\ +\ \zeta - k_o h)} \left\{ (e^{i\theta_1} \cos\zeta - i\ e^{i\theta_2} \sin\zeta)\underset{\sim}{p} + (-e^{i\theta_1} \sin\zeta - i\ e^{i\theta_2} \cos\zeta)\underset{\sim}{q} \right\}.$$

Different possibilities now arise depending on the orientation of the second quarter-wave plate and the analyzer. Only four will be considered.

Case 1: Quarter-Wave Plates Augment and the Polarizer-Analyzer are Parallel.

Let $\underset{\sim}{p}_3$ and $\underset{\sim}{q}_3$ give the axes of the second quarter-wave plate and $\underset{\sim}{p}_4$ the axis of the analyzer. Only the case when $\underset{\sim}{p}_4$ makes an angle of 45^o between $\underset{\sim}{p}_3$ and $\underset{\sim}{q}_3$ will be considered. Now, let the quarter-wave plates augment and the polarizer-analyzer be parallel,

i.e. $\underset{\sim}{p}_3 = \underset{\sim}{p}_2$, $\underset{\sim}{q}_3 = \underset{\sim}{q}_2$, $\underset{\sim}{p}_4 = \underset{\sim}{p}_1$:

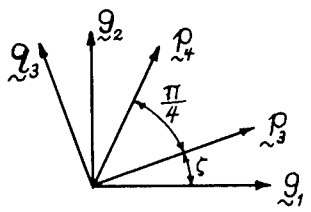

The wave transmitted by the quarter-wave plate is

$$\underset{\sim}{H} = A\, e^{i(\varphi + \zeta - k_o h)}\left\{(e^{i\theta_1} \cos\zeta - i\, e^{i\theta_2} \sin\zeta)\underset{\sim}{p}_3 + (-e^{i\theta_2} \cos\zeta + i\, e^{i\theta_1} \sin\zeta)\underset{\sim}{q}_3\right\} \tag{92}$$

The wave transmitted by the polarizer is given by

$$\underset{\sim}{H} = H\, \underset{\sim}{p}_4 \,, \tag{93}$$

$$H = A\, \frac{1}{\sqrt{2}}\, e^{i(\varphi+2\zeta-k_o h)}\left\{e^{i\theta_1} - e^{i\theta_2}\right\} \tag{94}$$

The real part is

$$R(H) = Q \cos(\varphi+2\zeta - k_o h + \epsilon) \tag{95}$$

where

$$Q = A\sqrt{2} \sin 2n\pi \,. \tag{96}$$

Thus, isochromatic lines give integer fringes. The isoclinics do not occur.

Case 2: Quarter-Wave Plates Opposed. Polarizer-Analyzer Crossed.

Consider the case when $\underset{\sim}{p}_3 = \underset{\sim}{q}_2$, $\underset{\sim}{q}_3 = -\underset{\sim}{p}_2$:

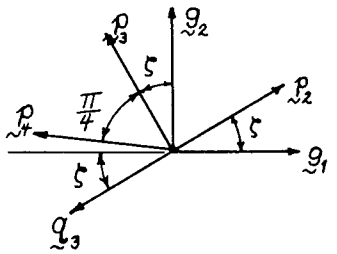

The wave transmitted by the quarter-wave plate is

$$\underset{\sim}{H} = A\, e^{i(\omega+\zeta - k_o h)}\Big\{(i\cos\zeta\, e^{i\theta_1} + \sin\zeta\, e^{i\theta_2})\underset{\sim}{q}_3 \qquad (97)$$

$$+ (-\sin\zeta\, e^{i\theta_1} - i\cos\zeta\, e^{i\theta_2})\, p_3\Big\}.$$

The wave transmitted by the polarizer is

$$H = A\,\frac{1}{\sqrt{2}}\, e^{i(\omega+2\zeta - k_o h + \frac{\pi}{2})}\Big\{e^{i\theta_1} - e^{i\theta_2}\Big\}. \qquad (98)$$

The real part is

$$R(H) = A\sqrt{2}\sin 2n\pi\ \cos(\omega+2\zeta - k_o h + \frac{\pi}{2} + \epsilon). \qquad (99)$$

In this case also, the isochromatic fringes are of integral fringe order.

Case 3: Quarter-Wave Plate Aligned. Polarizer-Analyzer Crossed.

The first two cases give a dark field in the absence of a model and yield integral order fringes.

By effectively rotating the analyzer, a light field is obtained which yields half-order fringes.

Consider the case $\underset{\sim}{p}_3 = \underset{\sim}{p}_2$, $\underset{\sim}{q}_3 = \underset{\sim}{q}_2$. The wave transmitted by the second quarter-wave plate is then

$$\underset{\sim}{H} = A\, e^{i(\varphi+\zeta-k_o h)}\Big\{(\cos\zeta\, e^{i\theta_1} - i\sin\zeta\, e^{i\theta_2})\underset{\sim}{p}_3 + (-i\sin\zeta\, e^{i\theta_1} + \cos\zeta\, e^{i\theta_2})\underset{\sim}{q}_3\Big\} \tag{100}$$

The wave transmitted by the analyzer is

$$H = A\frac{1}{\sqrt{2}}\, e^{i(\varphi-k_o h)}(e^{i\theta_1} + e^{i\theta_2}). \tag{101}$$

The real part is

$$R(H) = A\sqrt{2}\cos n\pi\cos(\varphi - k_o h + \epsilon). \tag{102}$$

Thus, dark lines correspond to prints for which n is an odd multiple of $\frac{1}{2}$.

Case 4: Quarter-Wave Plates Oppose. Polarizer-Analyzer Parallel.

Consider the case $\underset{\sim}{p}_3 = \underset{\sim}{q}_2$, $\underset{\sim}{q}_3 = \underset{\sim}{p}_2$. The wave transmitted by the analyzer has the real part:

$$R(H) = A\sqrt{2}\cos n\pi\cos(\varphi - k_o h + \frac{3\pi}{2} + \epsilon). \tag{103}$$

The isochromatic lines are again half-order fringes.

In each of the four cases the phase of the wave contains a factor ϵ which is determined by θ_1 and θ_2 but is not listed because it does not effect the fringe pattern.

4. BIREFRINGENCE.

4.1. Rheo-Optic Constitutive Relations.

The materials used in photo-mechanics are such that the dielectric tensor is a function of the history of strain. The material is isotropic, in the sense that response of a sample cut from a sheet is independent of the orientation of that sample. For small displacements, the relation will be linear:

$$K_{ij} = N_o^2 \delta_{ij} + \delta_{ij} \int_o^t \overline{A}(t-\tau)\dot{\epsilon}_{kk}(\tau)\, d\tau + \int_o^t 2\overline{B}(t-\tau)\dot{\epsilon}_{ij}(\tau)\, d\tau \,. \qquad (1)$$

In terms of the mean and deviatoric parts,

$$R_{ij} = K_{ij} - 1/3\ \delta_{ij}\ K_{rr},$$

the relation (1) has the form:

$$K_{rr} = 3\ N_o^2 + \int_o^t [3\overline{A}(t-\tau) + 2\overline{B}(t-\tau)]\dot{\epsilon}_{rr}(\tau)\, d\tau, \qquad (2)$$

$$R_{ij} = \int_o^t 2\overline{B}(t-\tau)\dot{e}_{ij}(\tau)\, d\tau \,. \qquad (3)$$

Using the stress-strain law of chapter 1, the entirely equivalent expression for the dielectric tensor in terms of stress history is found:

$$K_{rr} = 3N_o^2 + \int_o^t \overline{C}(t-\tau)\dot{\sigma}_{rr}(\tau)\, d\tau, \qquad (4)$$

$$R_{ij} = \int_o^t \overline{D}(t-\tau)\dot{s}_{ij}(\tau)\, d\tau, \qquad (5)$$

where

$$\overline{C}(t) = \int_o^t [3\overline{A}(t-\tau) + 2\overline{B}(t-\tau)]\, \dot{B}(\tau)\, d\tau\ , \qquad (6)$$

$$\overline{D}(t) = \int_o^t \overline{B}(t-\tau)\, \dot{J}(\tau)\, d\tau\ . \qquad (7)$$

The deviatoric part is especially important for the interpretation of the fringe order. The inverse of (5) will be important. It is

$$s_{ij} = \int_o^t \overline{E}(t-\tau)\, \dot{R}_{ij}(\tau)\, d\tau\ , \qquad (8)$$

where $\overline{E}(t)$ and $\overline{D}(t)$ are related by the integral equation discussed in section 2.9. These functions play an important role in photomechanics and will be given the names:

$\overline{D}(t)$ - optical creep function ,

$\overline{E}(t)$ - inverse optical creep function.

4.2. Stress and Strain Birefringence.

Consider the possibility

$$\overline{B}(t) = \overline{B}_o\, h(t)\ , \qquad (9)$$

where h(t) is the unit step function. Then

$$R_{ij} = 2\overline{B}_o \, e_{ij} \, , \tag{10}$$

$$\overline{E}(t) = \frac{1}{\overline{B}_o} \, G(t) \, , \tag{11}$$

$$\overline{D}(t) = \overline{B}_o \, J(t) \, . \tag{12}$$

In this case the deviatoric part of the dielectric tensor, and therefore the observed fringe order in a polariscope, is directly related to the strain. A material for which (9) holds may be termed <u>strain-birefringent</u>. The isoclinic angle then coincides with the principal axis of strain.

Consider the possibility

$$\overline{D}(t) = \overline{D}_o \, h(t) \, . \tag{13}$$

Then,

$$R_{ij} = \overline{D}_o \, S_{ij} \, , \tag{14}$$

$$\overline{B}(t) = \overline{D}_o \, G(t) \, , \tag{15}$$

$$\overline{E}(t) = \frac{1}{\overline{D}_o} \, h(t) \, . \tag{16}$$

Such a material may be called <u>stress-birefringent</u>. The fringe order then gives the difference in principal stresses and the isoclinic angle coincides with the principal axes of stress.

Consider an elastic material which is stress-birefringent. Combining the relations of section 2.2 with (13) - (16) leads to a relation of the form (10). Thus, a stress-birefringent elastic material is also strain-birefringent. Similarly, a strain-birefringent elastic material is also stress-birefringent.

Consider the possibility

$$\overline{D}(t) = a\, h(t) + \tfrac{1}{2}\, b\, J(t). \qquad (17)$$

where a and b are constants. Then,

$$R_{ij} = a\, s_{ij} + b\, e_{ij} \qquad (18)$$

Thus, the general expression includes the possibility that the fringe order depends on a combination of the stress and strain. The relation (18) is often in fair agreement with experiment.

The list of such special cases is endless. The relations obtained may describe some materials accurately enough for some applications, but they are certainly not universal. The relation (18) is particularly useful in qualitative reasoning, i.e., to exercises of "physical intuition".

4.3. Slow on Rapid Motion.

The constitutive relations (1) are of the same form as the stress strain laws of viscoelastic

materials. Thus, the same approximation theorems hold for both relations.

For sufficiently rapid straining, by (3),

$$R_{ij} = 2\,\overline{B}(0)\,e_{ij}\,. \tag{19}$$

The material is strain birefringent. Since, by (57) of chapter 2, the material is elastic under such straining, the material is also stress-birefringent.

For slow straining, by (3),

$$R_{ij} = 2\,\overline{B}(\infty)\,e_{ij}\,. \tag{20}$$

The material is strain-birefringent. Since, by (59) of chapter 2, the material is elastic for slow straining, it is also stress-birefringent.

4.4. Temperature Dependence.

Each of the material properties functions of section 4.1 is temperature dependent. From the experimental observations of the similarity of mechanical and optical creep, it may be expected that materials which are thermorheologically simple in their mechanical behavior are described by similar relations for the optical behavior.

Let the reduced time be defined by

$$\zeta(\tau) = \int_0^\tau b(T(t))\,d\tau\,.$$

The function b(T) of temperature may be termed the optical shift factor. An optically and thermo-rheologically simple material is then defined by the constitutive relation:

$$R_{ij} = \int_0^t 2\bar{B}(\zeta(t)-\zeta(\tau))\mathring{e}_{ij}(\tau)\, d\tau. \qquad (22)$$

This generalizes the relation(3).

It may happen that the mechanical and optical shift factors are the same. However, this must be determined experimentally.

5. BASIC FORMULAE FOR PLANE STRESS.

5.1. Normal Incidence.

Consider a slice of material of thickness h which experiences a state of plane stress described in section 2.4. The state of stress is to be determined by observing the isoclinic and isochromatic fringe patterns in a polariscope.

The fringe order n and the isoclinic angle δ are observed as a function of time. The results of chapter 3 are used to derive information about the dielectric tensor. Although the solution obtained there is exact only when K_{ij} is constant, it will be used here as an approximate solution when K_{ij} varies in both time and space. This approximation will be satisfactory as long as the time scale of the mechanical behavior is long compared to the time $\frac{Nh}{c}$, about 10^{-10} seconds; that is, the time required for light to traverse the model. The results of chapter 4 are then used to derive information about the stress tensor.

The x-y axis may be chosen arbitrarily. The principal axes of stress are then located at an angle ξ from the x toward the y axis:

$$\tan 2\xi = \frac{2\tau_{xy}}{\sigma_x - \sigma_y} = \frac{2s_{xy}}{s_x - s_y} . \qquad (1)$$

The principal stresses are given by

$$\sigma_1 = \sigma_x \cos^2\xi + \sigma_y \sin^2\xi + 2\tau_{xy} \sin\xi \cos\xi \ , \tag{2}$$

$$\sigma_2 = \sigma_x \sin^2\xi + \sigma_y \cos^2\xi - 2\tau_{xy} \sin\xi \cos\xi \ . \tag{3}$$

Thus,

$$\sigma_1 - \sigma_2 = (\sigma_x - \sigma_y) \cos 2\xi + 2\tau_{xy} \sin 2\xi \tag{4}$$

$$= (s_x - s_y) \cos 2\xi + 2s_{xy} \sin 2\xi \ . \tag{5}$$

Alternatively,

$$\sigma_x = \sigma_1 \cos^2\xi + \sigma_2 \sin^2\xi \ , \tag{6}$$

$$\sigma_y = \sigma_1 \sin^2\xi + \sigma_2 \cos^2\xi, \tag{7}$$

$$\tau_{xy} = (\sigma_1 - \sigma_2) \sin \xi \cos \xi \ . \tag{8}$$

Thus,

$$s_x - s_y = \sigma_x - \sigma_y = (\sigma_1 - \sigma_2) \cos 2\xi \ , \tag{9}$$

$$s_{xy} = \tau_{xy} = \tfrac{1}{2} (\sigma_1 - \sigma_2) \sin 2\xi \ . \tag{10}$$

Equations (1) to (10) are simple consequences of the tensor character of the stress tensor σ_{ij}. Similar relations hold for the dielectric tensor.

Let ζ denote the angular orientation of the principal axis of K_{ij} in the plane. Then,

$$R_x - R_y = K_x - K_y = (K_1 - K_2) \cos 2\zeta \ , \tag{11}$$

$$R_{xy} = K_{xy} = \tfrac{1}{2}(K_1 - K_2) \sin 2\zeta \ . \tag{12}$$

By (42) of section 3.5,

$$R_x - R_y = \frac{N_o^2 c}{\omega h} (P_1 - P_2) \cos 2\zeta \ , \tag{13}$$

$$R_{xy} = \tfrac{1}{2} \frac{N_o^2 c}{\omega h} (P_1 - P_2) \sin 2\zeta \ . \tag{14}$$

By (51) and (52) of section 3.5,

$$R_x - R_y = \frac{4\pi N_o c}{\omega h} n \cos 2\zeta \ , \tag{15}$$

$$R_{xy} = \frac{2\pi N_o c}{\omega h} n \sin 2\zeta \ , \tag{16}$$

and n is the isochromatic fringe order .

By (5) of section 4.1,

$$n \cos 2\zeta = \int_o^t \Psi(t-\tau) \frac{d}{d\tau} [(\sigma_1(\tau) - \sigma_2(\tau)) \cos 2\xi(\tau)] d\tau, \tag{17}$$

$$n \sin 2\zeta = \int_o^t \Psi(t-\tau) \frac{d}{d\tau} [\sigma_1(\tau) - \sigma_2(\tau)) \sin 2\xi(\tau)] d\tau; \tag{18}$$

where,

$$\Psi = \frac{\omega h}{4\pi N_o c} \overline{D} \ . \tag{19}$$

By (8) of section 4.1,

$$(\sigma_1-\sigma_2)\cos 2\xi = \int_o^t \Phi(t-\tau)\frac{d}{d\tau}[n(\tau)\cos 2\zeta(\tau)]\,d\tau, \quad (20)$$

$$(\sigma_1-\sigma_2)\sin 2\xi = \int_o^t \Phi(t-\tau)\frac{d}{d\tau}[n(\tau)\sin 2\zeta(\tau)]\,d\tau; \quad (21)$$

where,

$$\Phi = \frac{4\pi N_o c}{\omega h}\bar{E}\,. \quad (22)$$

Equations (20) and (21) can be used to determine the difference in principal stresses and the orientation of principal axes of stress at a point from the observed history of fringe order and isoclinic angle at the point with normal incidence of light.

The principal axes of stress and strain coincide with the isoclinic angle if and only if the isoclinic angle is constant. Otherwise all three sets of principal axes are different.

When the isoclinic angle is independent of time, the equations (20) and (21) give the result:

$$\sigma_1-\sigma_2 = \int_o^t \Phi(t-\tau)\,\dot{n}(\tau)\,d\tau\,. \quad (23)$$

Inversely

$$n = \int_o^t \Psi(t-\tau)\frac{d}{d\tau}[\sigma_1(\tau)-\sigma_2(\tau)]d\tau\,. \quad (24)$$

5.2. Oblique Incidence.

The observation of the history of the fringe pattern with the incident light directed normal to the slice gives the difference in principal stresses and the orientation of the axis of principal stress. The values of the two principal stresses are, therefore, not determined solely by the observation of fringe order and isoclinic angle at a point with normal incidence.

If the principal axes of stress are found to have the same orientation at all times, then the method of oblique incidence can be conveniently used to give a third independent piece of information: From the combined observations with normal and oblique incidence the two principal stresses can be calculated. If the principal axes of stress are not independent of time the method of oblique incidence can still be used but the relations are more complicated and will not be given in this paper.

The z-axis is normal to the slice and the x,y-axes are taken along the principal axes of stress. The case when the principal axes of stress do not change with time will be considered. By (5) of section 4.1, the principal axis of K_{ij} do not rotate. Thus, the x, y-axes are principal axes of the dielectric at all

times. As an example, suppose that the incident light is directed normal to the y-axis and making an angle α with the z-axis. The fringe order can be related to the dielectric tensor by (72) - (74) of section (3). The dielectric tensor is related to the stress tensor by (4) and (5) of section 4. Combining these relations for the case when the x,y-axes are the principal axes of both stress and dielectric tensors leads to the relations.

$$n = \int_o^t \dot{\psi}(t-\tau) \left[\dot{\sigma}_1(\tau) \cos^2\beta - \frac{\dot{\sigma}_2(\tau)}{\cos\beta}\right] d\tau \ . \qquad (25)$$

Where, again,

$$\sin\beta = \frac{1}{N_o} \sin\alpha \ ,$$

$$\Psi = \frac{\omega h}{4\pi N_o c} \overline{D}.$$

The inverse relation is

$$\sigma_1 \cos^2\beta - \frac{\sigma_2}{\cos\beta} = \int_o^t \Phi(t-\tau)\, \dot{n}(\tau)\, d\tau, \qquad (26)$$

$$\Phi = \frac{4\pi N_o c}{\omega h} \overline{E} \ .$$

6. PREPARATION OF MODEL MATERIAL.

It is usually desired to determine the stress in a viscoelastic solid from observations on a geometrically similar model. The experimental procedure determines the stresses in the model. The correlation with the prototype generally requires that the viscoelastic properties of the model be similar to those of the prototype: The Poisson's ratio in creep $\nu(t)$ must be the same and the tensile creep compliances must be proportional for the model and prototype materials. Differences in Poisson's ratio do not generally lead to significant errors. The compliances are always proportional for elastic materials; and so, the choice of model material does not present a problem in photoelasticity.

It is generally necessary to manufacture a new material for each viscoelastic experiment. One such material is described in this section. Many other materials could be used.

An epoxy mixture made from components manufactured by the CIBA Co. can be made to give considerable variation in viscoelastic properties. The material described here is made of CIBA Araldite 502,508, and 963, in the proportions 45/45/10. Two different batches referred to as A and B, having the same formula, are described.

A mold is prepared to cast sheets of the material $\frac{1}{4}$ inch thick and two square feet in area: Sheets of plate glass are

used for the two faces of the mold, $\frac{1}{4}$ inch surgical tubing forms a gasket between the sheets on three sides, the thickness is controlled by $\frac{1}{4}$ inch spacers placed between the glass faces and outside of the gasket.

This epoxy formulation is a very tenacious adhesive and care must be taken to insure mold removal: The surfaces must first be cleaned with a solvent. Three light coats of a Carnuba-base wax are then applied, allowing each coat to partially dry and polishing it before application of the next coat. Finally all surfaces are sprayed with a polyvinyl alcohol solution which when properly applied and dried forms a smooth water soluble film. Some experience is required to evolve a spraying technique which gives a glassy smooth surface. The Carnuba base wax and the polyvinyl alcohol solutions are available through most commercial fiberglass supply houses.

At room temperature the viscosity of the uncatalyzed resin components is such that small air bubbles will become trapped in the mixture while stirring, resulting in a poor casting. If the mixture is placed in a vacuum some bubbles will be drawn out but the mixture will catalyze before all of the bubbles are gone. However, if the resin components are heated to 130°F prior to mixing the viscosity is lowered sufficiently to allow entrained air to float off before

solidification. Heating the components reduces the pot life of the mixture to less than five minutes after the hardener is added. Final mixing and pouring into the mold must be done quickly. A paddle mounted at the end of a rod and driven by a slow speed drill motor facilitates mixing.

The resin is cured in an oven for 12 hours while the temperature is maintained at 160 ± 5°F. The mold is taken from the oven and the clamps removed. The rubber-tube gasket is stripped off and a razor blade is used to cut around the edges between the cast sheet and the glass. Wooden wedges are slowly pressed between the edges of the glass faces while the sheet is held under running water.

Careful prying will remove the mold after about five or ten minutes. The newly cast sheet is washed to remove the mold release agent and placed on a flat paper or teflon coated surface to relax to equilibrium.

After the sheet has relaxed for a day, models and specimens may be laid out on the sheet. These shapes are cut from the sheet on a band saw at high speed with a skip-tooth blade.

Machining accurate models from this material presents some problems. If the material is clamped lightly in a vice or a chuck it relaxes and becomes loose. If the vice or chuck is tightened enough to hold the part, the part becomes distorted so that a flat surface or a square edge after removal from the jig is no longer flat or square. Another

difficulty appears when a heavy cut is made: The tool mashes the material under it slightly so that after relaxation the part is larger than expected.

These difficulties have been overcome by using double-sided adhesive tape to hold the model to the face plate for turning operations and by taping the jaws and bottom of the vice for milling operations. If sharp corners are required, the model may be taped on both faces and sandwiched between 1/8 inch plexiglas, the sandwich being then taped on both edges and very lightly clamped in a vice. If a particular dimension is desired, it should be approached slowly with fine cuts. When the machine has reached the final setting, the specimen is allowed to relax for 15 to 30 minutes and the last cut is made at the same machine setting. This process can be repeated if extreme accuracy is required.

Flat surfaces and edges are cut with a sharp fly cutter running at high speed. Circular section can be turned in a lathe at high speed using a sharp pointed tool with about 35° rake. Holes may be drilled if the model is sandwiched between plexiglas and the drill is sharp and turned at high speed.

For some models it is helpful to cool the model in a refrigerator immediately before machining. The material is quite stiff at 40°F.

The models have been machined dry. If a coolant is to be

used, experiments should be made to determine if the coolant accelerates the growth of edge fringes. Water, for example, will considerably accelerate the growth of edge fringes.

Finished models stored at normal room conditions will be useable for several weeks or more before edge fringes become excessive. Carnuba wax, acetone, n-heptane, methylenedichloride and water will accelerate edge fringe growth. A dessicating atmosphere will retard edge fringe growth.

The photoviscoelastic material is calibrated in a tensile creep test. A typical tensile specimen $\frac{1}{4}$" thick by 0.6" long is shown in Fig. 1. Usually six or eight calibration specimens are cut from each sheet of model material. Experiments have shown that specimens cut from different locations and orientations in the sheet yield the same creep behavior.

The entire batch of specimens may be stacked on edge and milled to a uniform width in one set-up with a fly cutter. Aluminum tabs are bonded to each end of each specimen with Eastman 910 and the specimens are placed on edge on a flat surface to relax before testing. By having six or eight specimens any one specimen has enough time to relax between tests while the other specimens are tested.

7. MATERIAL CHARACTERIZATION.

7.1. Creep Test.

The mechanical and optical properties are determined by the tensile creep test: A constant uniaxial stress is applied and the strain and birefringence are recorded, figure 2. The load is applied to the specimen by releasing a weight and total change in length is measured with a differential transformer. The load is measured with a beam instrumented with strain gages. The time interval during loading is approximately 0.2 seconds. A calibrated clip gage, made by bending a 0.010 inch thick strip of aluminum and instrumenting it with strain gages, is used to measure the changing width of the specimen as it creeps.

All strain gages and differential transformers are powered by, and their outputs recorded on, a 6-channel Brush recorder with a calibrated time base.

The fringe growth is also automatically recorded: The output of a mercury-arc lamp is filtered with a Wratter 77A filter which passes the green line (5460 $\mathring{A}$) of mercury. This light is passed through a polarizer (Polaroid), through the creep test specimen, through a second polarizer with axis at right angles to the first and then into a photomultiplier tube. The output of the photomultiplier tube shows the periodic

increasing and decreasing of light intensity. The maximums and minimums of this curve are well defined and represent increasing integral fringe orders.

The model is enclosed in a box which has electric resistance heaters, automatically controlled to maintain a set temperature ± 0.2°F over the range from room temperature to 150°F. Circulating fans within the test chambers insure a uniform temperature.

The glass transition temperature for the model material is in the region of room temperature. Small changes in temperature (5°F) cause marked changes in mechanical behavior. At 130 to 150°F the relaxation time is very short and the material is rubbery while at 32°F it is quite rigid.

For the tensile creep test, the principal axes of stress, strain, and refraction coincide. Let σ denote the tensile stress . Equation (24) of section 5.1 leads to

$$\psi(t) = \frac{n(t)}{\sigma} \quad . \tag{1}$$

From (12) of section 2.1,

$$D(t) = \frac{\epsilon_x(t)}{\sigma} \quad . \tag{2}$$

From (13) of section 2.1,

$$\nu(t) = - \frac{\epsilon_y(t)}{\epsilon_x(t)} \quad . \tag{3}$$

Then J(t) and B(t) can be calculated from (16) and (17) of section 2.1.

$$J = 2(1+ \nu)\, D, \tag{4}$$

$$B = 3(1- 2\nu)\, D. \tag{5}$$

The constant stress σ is taken to be the load divided by the undeformed cross-section area. The successive peaks on the light intensity curve correspond to integer values of the fringe order n. By observing the time of occurrence, the optical creep function $\psi(t)$ can be determined from (1). A graph of ψ determined at room temperature for mix A is shown in Fig. 3. The results of tests at various temperatures are shown in Fig. 4. for mix B. These two mixes were of the same proportions of raw material but show a slight difference in their mechanical and optical properties.

The longitudinal strain was taken to be the total change in length divided by the original length. The tensile creep compliance D(t) computed by (2) is shown in Fig. 5, and the transverse contraction ratio $\nu(t)$ is shown in Fig. 6. Because of the small change in thickness the lateral strains are difficult to measure, and the large band of experimental data in Fig. 6 is due to this experimental error rather than any real

variation of material properties. The shear creep compliance J(t) and bulk creep compliance B(t) calculated from (4) and (5) are shown in Fig. 7 and 8. In the tests at higher temperatures of mix B, only the longitudinal strain was measured. The tensile creep compliance is shown in Fig. 9.

If the dependence of the final data on temperature is neglected in Fig. 4, then the temperature dependence of the creep functions over this small change of temperature can be reasonably well described by a temperature shift factor. The optical and mechanical shift factors are shown in Fig. 10.

The optical creep function is also reasonably well described by the empirical relation (18) of section 4.2 with $a = 18.4 \times 10^{-3}$ in/lb^2 and $b = 36.8$. The resulting error is 20% for some ordinates.

In order to analyze the photoviscoelastic data it is necessary to calculate the inverse of the optical creep function $\psi(t)$ related to $\Phi(t)$ by

$$\int_0^t \Phi(t)\ \psi(t-\tau)\ d\tau = t.$$

This equation is solved by a numerical technique in conjunction with the digital computer as described in section 2.9. The results are shown in Fig. 11 for one case.

7.2. Thermal Properties.

The coefficient of thermal expansion was measured in the jig shown in Figure 12. The specimen rests on a Teflon-coated surface of the jig and one end is bonded to the jig. A metal tab is bonded to the free end of the specimen and a fine wire soldered to the tab leads to one terminal of an ohmmeter. The ohmmeter registers a short circuit when the micrometer is brought to touch the free end of the specimen. By using this system the micrometer measurements may be repeated to within ± 0.0002. Such accuracy cannot be obtained by mechanical feel due to the low modulus of the model material.

The jig was placed in an oven, allowed to come to equilibrium at several temperatures and changes of length were measured. The hysteresis was determined by approaching a given temperature from above and below and was small. The temperature was varied between 70 and 110°F and the coefficient of thermal expansion was calculated to be $1.06 \times 10^{-4} \frac{\text{in}}{\text{in} - {}^{\circ}\text{F}} \pm 6\%$. Correction was made for the expansion of the measuring jig.

The coefficient of thermal diffusivity was calculated by measuring the temperature history at the centers of two slugs immersed in a constant temperature bath. The temperatures were measured with iron-

constantan thermocouples cast into the slugs. The constant temperature bath was water in a large laboratory thermos bottle.

The slugs and the bath were allowed to reach their separate equilibrium temperatures as determined by the thermocouple readings. The slugs were then immersed in the bath and stirred vigorously. The temperature history being recorded on a calibrated, self-balancing potentiometer. A rectangular and a cylindrical slug were each tested several times to insure reproducibility. The thermal diffusivity was calculated for both geometries at several points in the temperature history and was 32.9×10^{-4} ft^2/hour ± 4%.

The specific heat was determined by a calorimeter test and was 0.503 BTU/lb$^{\circ}$F ± 8%. The density of the model material is 0.046 lb/cubic inch. From these values the thermal conductivity was computed to be 0.131 BTU/hr ft$^{\circ}$F ± 10%.

SHEAR TEST.

8.1. Specimen and Apparatus.

A sheet was bonded to metal blocks along opposite edges as shown in Fig. 13. A state of nearly plane stress is obtained in the sheet by loading the blocks. If the load on the block is constant, the problem is one of proportional loading as described in section 2.3. The stresses will be constant if the time variation of Poisson's ratio can be neglected. Experience with elasticity problems indicates that the observed variation of ν should not have a significant effect on the stress state. Therefore this configuration was chosen for some preliminary tests.

The polariscope used is shown in Fig. 14. It is a versatile piece of equipment for general use in photoviscoelasticity. It differs from the ordinary photoelastic bench in that the polarizer-analyzer combination can be rapidly rotated by electric motors.

Three light sources may be used: a point source (d.c. mercury arc with a Wratten 77A filter), a distributed source (a.c. mercury arc and a green fluorescent), and diffused source. Condensing lenses are used with the point source light to get parallel beam through the specimen. The lenses are removed from the light path when the distributed light sources are used.

Each lens stand is fitted with a ball-bearing carrier to support the rotating polaroid around its outside edge. The polaroid is driven by a stepping solenoid through a positive drive, link chain. When the solenoid is pulsed the polaroid advances 9°. The pulse rate is continuously adjustable from 5 pulses per second to 1 pulse per 2 minutes.

A 16 mm Cine Special camera is used to record the fringe patterns. Mounted next to the model and in the field of view of the camera is a digital timer with 1/10 second minimum reading. Incorporated in the timer is a numbered wheel driven by a small rotating solenoid which is tied to the driver solenoids and indicating the angle of the polarizing axes.

During the first minute after loading the camera is run at 16 frames per second to capture the rapidly changing fringe pattern. The frame rate is then reduced to 1 frame per second. As the fringe patterns approach equilibrium the frame rate is correspondingly reduced.

A model is mounted in grips in the loading frame and the upper grips are connected to a load cell through a universal joint. Two load cells of differing sensitivities are available. Four loading patterns may be used: constant load, constant strain, constant strain

rate and sinusoidal strain.

Constant loads are applied by hanging weights on the specimens and constant strains are applied by using a heavy weight to force the loading mechanism against a present stop. Constant strain rate is applied to the model by driving the lower grips with a 220 volt, 3 phase motor operating through a gear change set. By changing the gears the strain rate may be varied between 0.0418 and 5.75 inches/minute. A spring loaded can and tappet mechanism supplies the sinusoidal strains, Figure A.6.2. The mechanism is driven by an electric motor through a Zeromax speed reducer. The frequency is continuously variable from 0 to 400 cycles/minute and the maximum amplitude may be varied between 0 and 0.2 inches, by inserting appropriate cans. All of the loading mechanisms are mounted in a rigid frame. Strains are measured with differential transformers and read out on a Brush recorder or an oscilloscope equipped with a camera.

8.2. Creep in Shear.

In the first test, the model was "sheared" by constant loads P_1. As shown in Section 2.3, if the variation in ν is neglected, the stress will be constant and be the same as if the material were elastic. The

stress state in an elastic material was determined by standard photoelastic means. It was found that the shear stress varied along the centerline as shown in Fig. 15. By symmetry, the point in the center of the specimen experiences a pure shear stress, i.e. $\sigma_x = \sigma_y = 0$. Thus, constant loads P_1 are expected to give a constant state of stress

$$\begin{aligned} \sigma_x &= 0 , \\ \sigma_y &= 0 , \\ \tau_{xy} &= \tau , \end{aligned} \tag{1}$$

at the center. The particle at the center experiences a creep test. By the formula of Section 5.1, the expected value of fringe order is

$$n(t) = 2\tau\, \psi(t) . \tag{2}$$

The experimental results are shown in Fig. 16. They agree with the expected value. The small deviation is thought to be due to the large shear strains which may exceed the range of linear behavior.

8.3. Rotation of Principal Axes.

It was then decided to demonstrate the fact that the isoclinic angle does not coincide with the principal axes of stress. By first applying a load P_2 and then,

at a later time t_o, applying the load P_1, the principal axes of stress can be made to rotate. The isoclinic angle can be simultaneously measured.

The weight of the frame alone caused some shear stress which may be regarded as having reached an equilibrium state. By (5) of section 4.1,

$$R_{xy} = \overline{D}(\infty)\ \tau_o\ ,$$
$$R_x - R_y = 0\ , \tag{3}$$

where $\tau_o = 0.30$ psi.

The loads P_2 result in a state of stress at the center with $\tau_{xy} = 0$. The stresses σ_x and σ_y determined by photoelasticity using oblique incidence were:

$$\sigma_x = 1.95\ P_2,$$
$$\sigma_y = 0.22\ P_2, \tag{4}$$
$$\tau_{xy} = 0.$$

Thus

$$R_{xy} = 0\ ,$$
$$R_x - R_y = \overline{D}(t)(\sigma_x - \sigma_y). \tag{5}$$

The shear load P_1 applied at time t_o results in stresses:

$$\begin{aligned} \tau_{xy} &= \tau \ , \\ \sigma_x &= 0 \ , \\ \sigma_y &= 0 \ . \end{aligned} \tag{6}$$

From the photoelastic test $\tau = 2.5\ P_1$.

Thus,

$$\begin{aligned} R_{xy} &= \overline{D}(t-t_o)\ \tau \ , \\ R_x - R_y &= 0 \ . \end{aligned} \tag{7}$$

Since the problem is linear, the response to the three stress states can be superimposed. The combined values of the tensor R_{ij} for $t > t_o$ are determined by adding (3), (5), and (7):

$$\begin{aligned} R_{xy} &= \overline{D}(\infty)\ \tau_o + \overline{D}(t-t_o)\tau \\ R_x - R_y &= \overline{D}(t)\ \sigma \ . \end{aligned} \tag{8}$$

The isoclinic angle is given by

$$\tan 2\zeta = \frac{2R_{xy}}{R_x - R_y} \tag{9}$$

Thus,

$$\tan 2\zeta = \frac{\bar{D}(\infty)}{\bar{D}(t)} \frac{2\tau_o}{\sigma_x-\sigma_y} + \frac{\bar{D}(t-t_o)}{\bar{D}(t)} \frac{2\tau}{\sigma_x-\sigma_y}$$

$$= \frac{\psi(\infty)}{\psi(t)} \tan 2\xi_o + \frac{\psi(t-t_o)}{\psi(t)} \tan 2\xi \qquad (10)$$

The angle ζ predicted by (10) is compared with the observed isoclinic angle in Fig. 17. The agreement is within experimental error.

9. CIRCULAR DISK.

9.1. Specimen and Apparatus.

Typical models are shown in Fig.18 and Fig. 19. The outer boundary is circular but the inner boundary may be an irregular shape. The model may be heated along the inner boundary and loaded by a uniform pressure along the outer boundary.

The loading jig is pictured in Fig. 20. Pressure is applied through a 0.010" thick latex diaphragm. The diaphragm is designed to have enough slack to follow the model as it deforms without stretching thus maintaining uniform pressure.

The uniformity of the loading and the pressure efficiency of the diaphragm were determined with the elastic, Hysol 4485 specimens pictured in Fig. 19. Knowing the elasticity solution for the circular disk and the photoelastic fringe constant for the calibration model material one may calculate the effective pressure acting on the model. This compared to the gage reading of the air pressure acting on the diaphragm establishes the pressure efficiency of the jig. Non-uniformity in the pressure around the edges of the disk will cause the fringe pattern to depart from concentricity. A measure of this non-uniformity is the per cent variation in fringe order around an imaginary

concentric circle drawn on the model. A picture of a loaded calibration specimen is shown in Fig. 21. The pressure is uniform to within 10% and the jig efficiency (effective pressure/gage pressure) is 68%.

The model is sandwiched in the jig between two $\frac{1}{4}$" Plexiglas guards. Polaroid is bonded to the model side of each guard. These guards are not loaded. They serve to contain the thin latex diaphragm, to prevent the low modulus model from buckling, and to insulate the heated model. A copious layer of thin oil separates the model from the guards. Calibration tests show that the friction is insignificant.

The model is heated along the inner edge by a resistance wire heater fitted into the opening. In the tests conducted, the model was heated to an equilibrium temperature and a preliminary test was run to determing the temperature distribution. A dummy model and guard of the same materials and dimensions as the test model and guard were placed in the loading jig. Holes 0.020" in diameter were drilled through the guard and into the model at several stations. These holes were filled with oil to minimize their effect on the temperature distribution. The model was heated to equilibrium with constant power input to the heater. A small iron-

constanan thermocouple probe was placed sequentially into the holes to measure the temperature. Several tests showed that the temperature distribution could be repeated to within ± 1°F. The model and apparatus used for this test is shown in Fig. 22.

9.2. Exterior Pressure.

The model of Fig. 18 was loaded with a step input (approximately 0.1 second rise time) of pressure which was maintained constant. The changing fringe patterns were recorded on a 16 mm movie camera running at 16 frames per second, shown in Fig. 23.

It was shown in Section 2.4 that the stress field in a plane stress problem with stress boundary conditions and uniform temperature is the same as if the material were elastic. In particular, the stress is independent of the material properties. Thus, if the unheated model is subjected to constant external pressure β, the stress at any point should be constant: Each particle experiences creep at constant stress. The isoclinic angle at each point is then constant and coincides with the principal axes of stress. With the coordinate axes along the principal axes, equation (24) of section 5.1 leads to

$$n(t) = \psi(t) [\sigma_1 - \sigma_2] . \qquad (1)$$

Since $\psi(t)$ is known from the tensile test, the expected fringe order can be calculated, to within a constant factor.

The actual fringe pattern was recorded with a movie camera. A typical frame is shown in Fig. 24. The expected fringe order is compared with the observed fringe order at several points in Fig. 25, and the agreement is satisfactory. The stress is constant and the stress at the star root, point A, is found to be 41 psi or 3.9 p. This agrees with the photo-elasticity solution.

9.3. Exterior Pressure with Temperature Gradient.

The model was heated until a steady non-uniform temperature distribution was reached. This temperature was maintained throughout the loading. Thus each particle experiences isothermal deformations. The relations of section 5.1 apply to each point but the function ψ will be different for each point because the temperature is different.

It was expected that the stress at the inner boundary due to a step change in boundary pressure would be large at first, then diminish, but finally increasing towards the initial value: As shown in Section 2.5, the initial stress should be the same as

for an elastic material and therefore, neglecting the effect of temperature on the value of G(o) and K(o), the stress should be the same as in the uniform temperature test. The hotter points on the inner boundary then begin to relax. The modulus G(t) becomes much smaller at the hotter points. Consequently, they "carry a smaller portion of the load", and the stress will decrease at the hotter points. As described in Section 2.6, the stress at long times is the same as for an elastic material; therefore, neglecting the effect of temperature on G(∞) and K(∞), the stress should approach that observed in the uniform temperature test.

The fringe order actually observed at a point is shown in Fig. 26. At a point on the boundary the principal axis of stress is normal to the boundary at all times. The only non-zero stress is tangent to the boundary. Choose the coordinate axes along the principal axes of stress. Then (23) of section 5.1 applies:

$$\sigma = \int_o^t \Phi(t-\tau)\, \dot{n}(\tau)\, d\tau \qquad (2)$$

The stress calculated using the observed fringe order and the function $\Phi(t)$ calculated from the optical creep function $\psi(t)$ for the particle temperature, is shown in Fig. 27. It has the expected character. The

exact analytical solution is unknown and so no comparison is possible.

ACKNOWLEDGEMENTS: This report was prepared as a part of a project sponsored by the National Aeronautics and Space Administration, Research Grant NsG-401, with the University of Washington. The project is directed by Professor R.J.H. Bollard. The analytical work in this report is due mainly to the first author while the experimental work is mainly due to the second author. Mr. Peravali Ramanaiah developed the numerical program for solution of the integral equations and data processing.

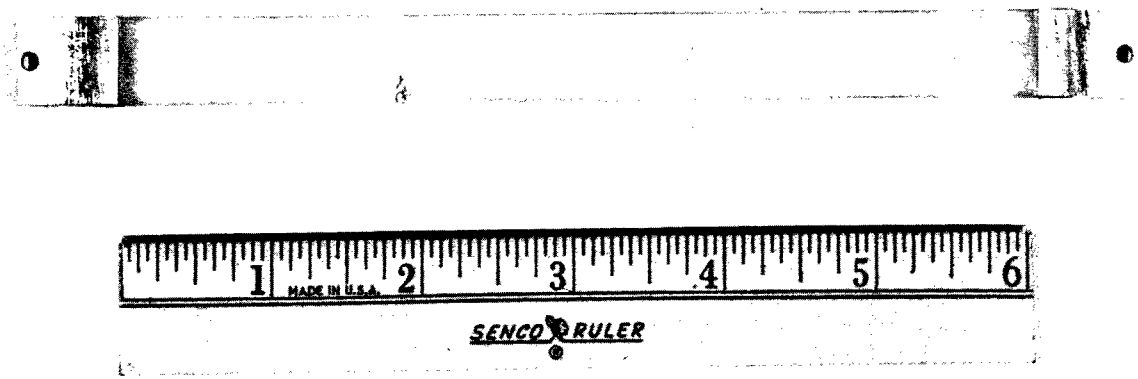

Figure 1. Tensile creep specimen.

(a) loading frame
(b) light source, filtered Hg arc
(c) Polarizer and 1/4 λ plate
(d) tensile specimen
(e) analyzer and 1/4 λ plate
(f) photomultiplier tube
(g) Brush recorder
(h) thermoelectric coolers
(i) power supply and control for coolers

Figure 2. Tensile calibration bench.

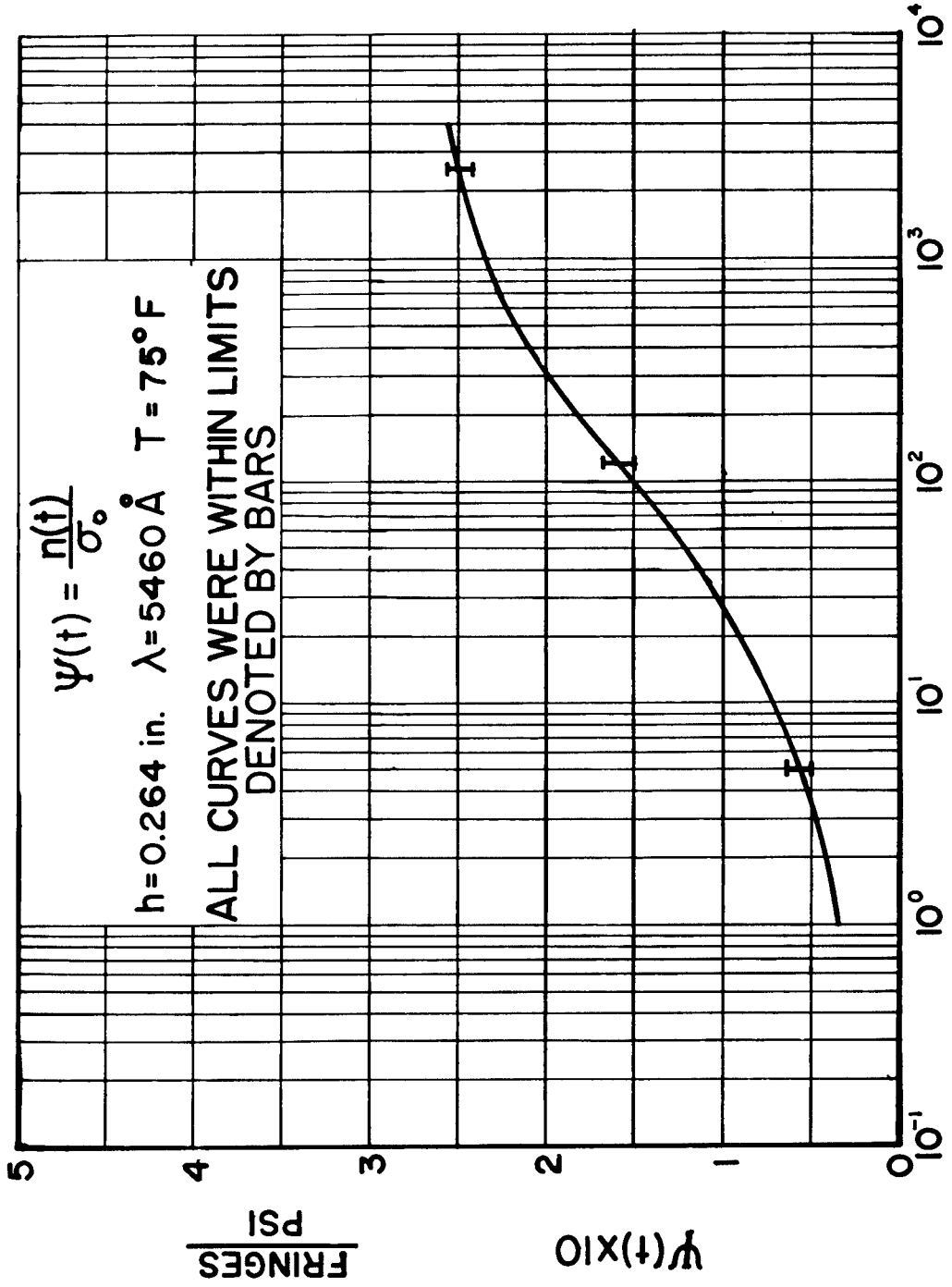

Figure 3. Optical creep compliance Mix A.

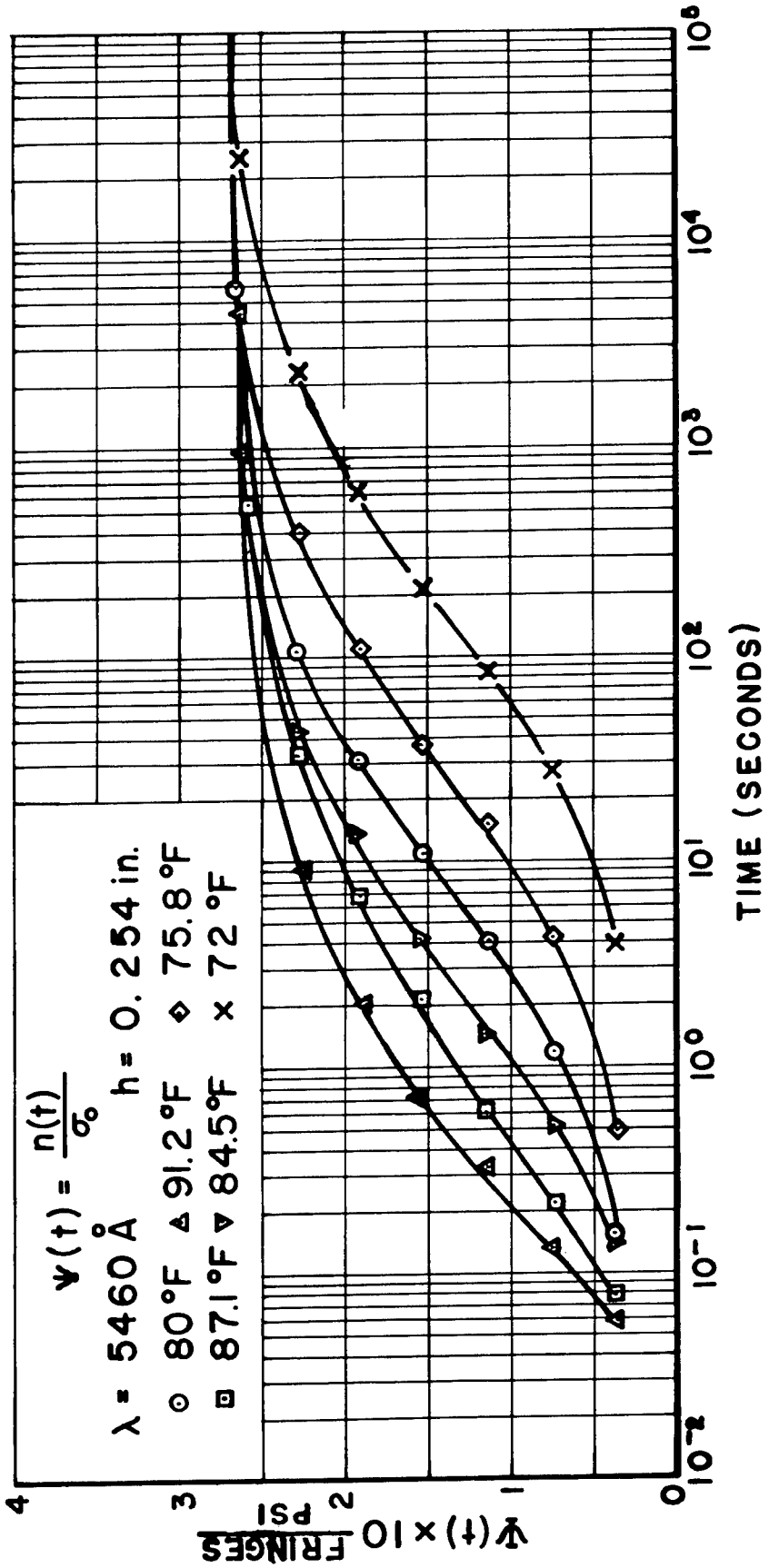

Figure 4. Optical creep compliance Mix B.

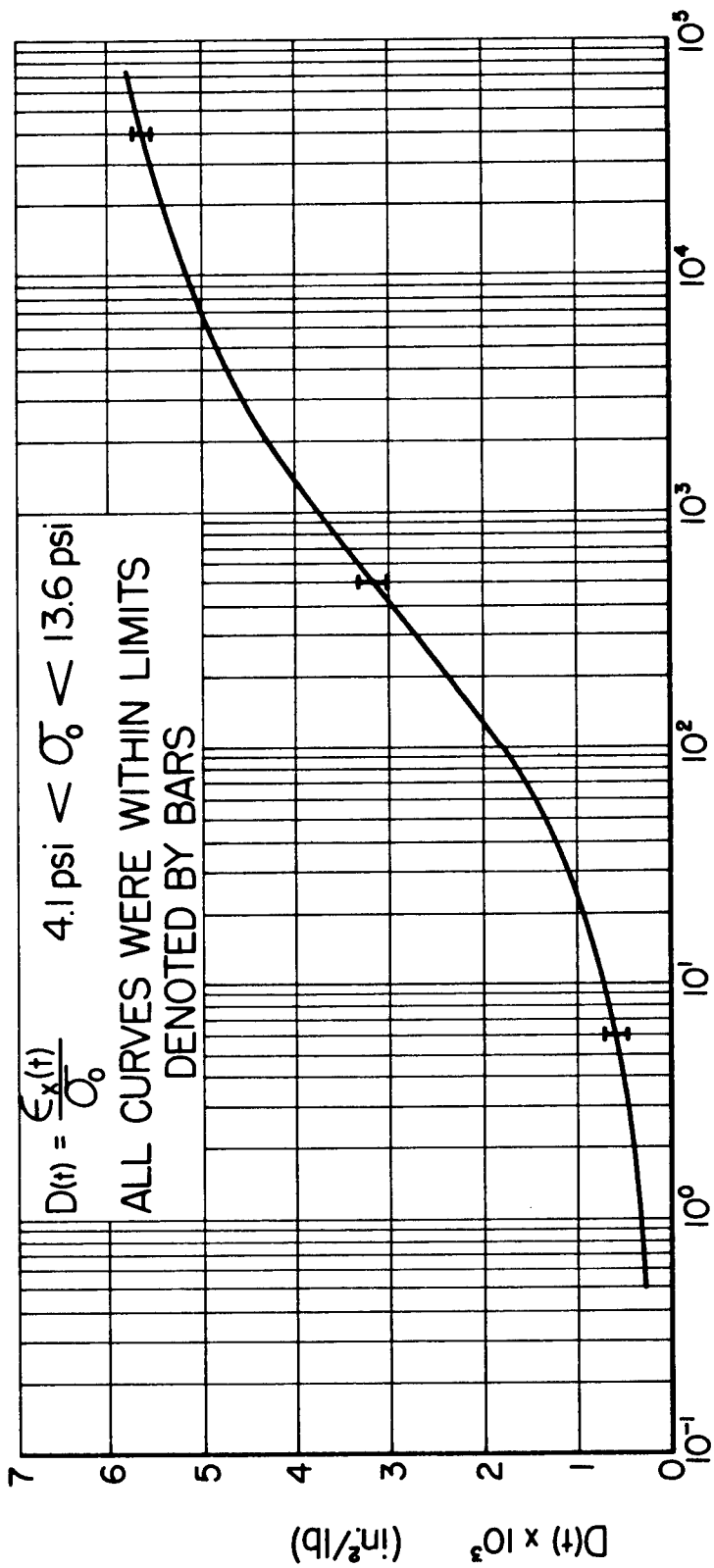

Figure 5. Tensile creep compliance, Mix A.

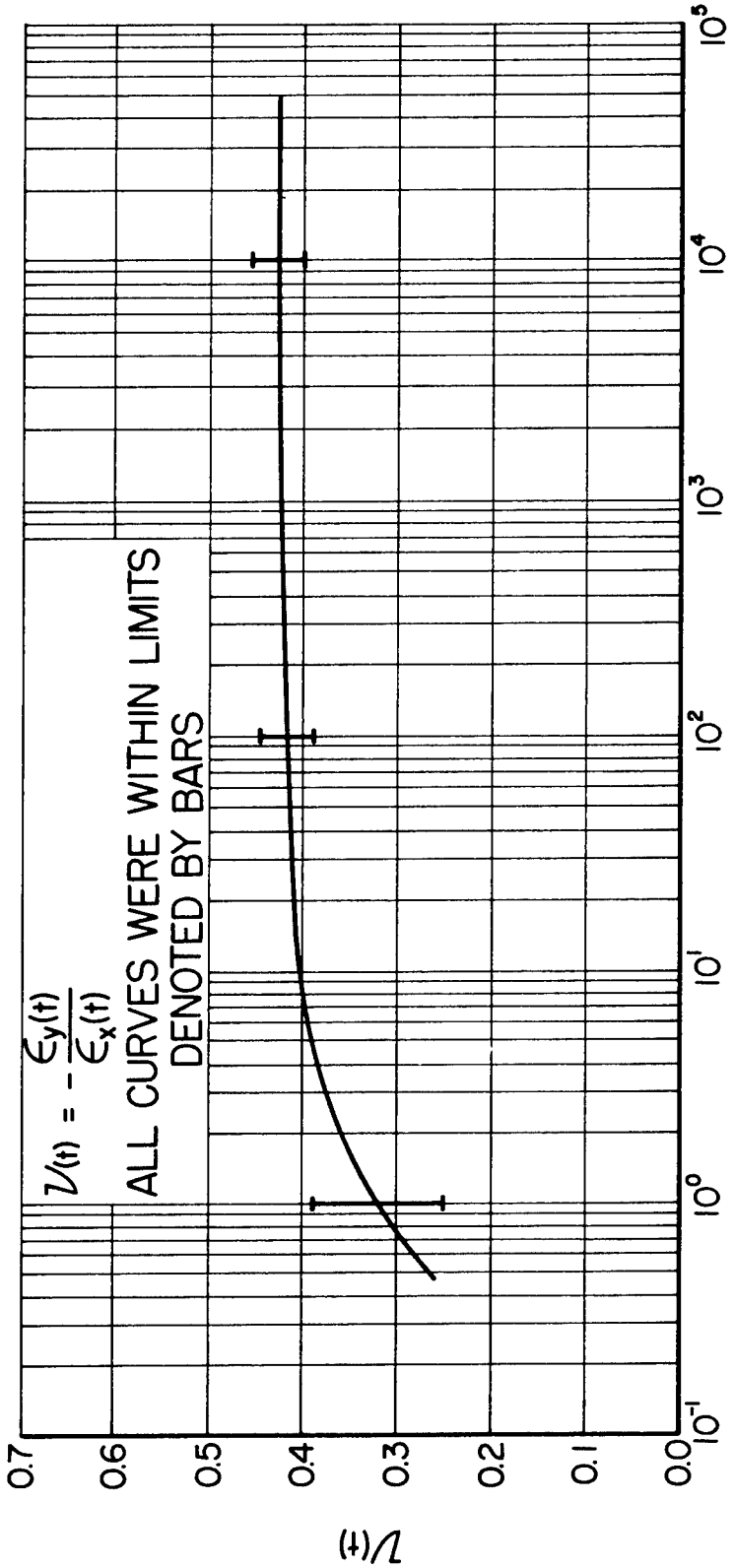

Figure 6. Poisson ratio in creep, Mix A.

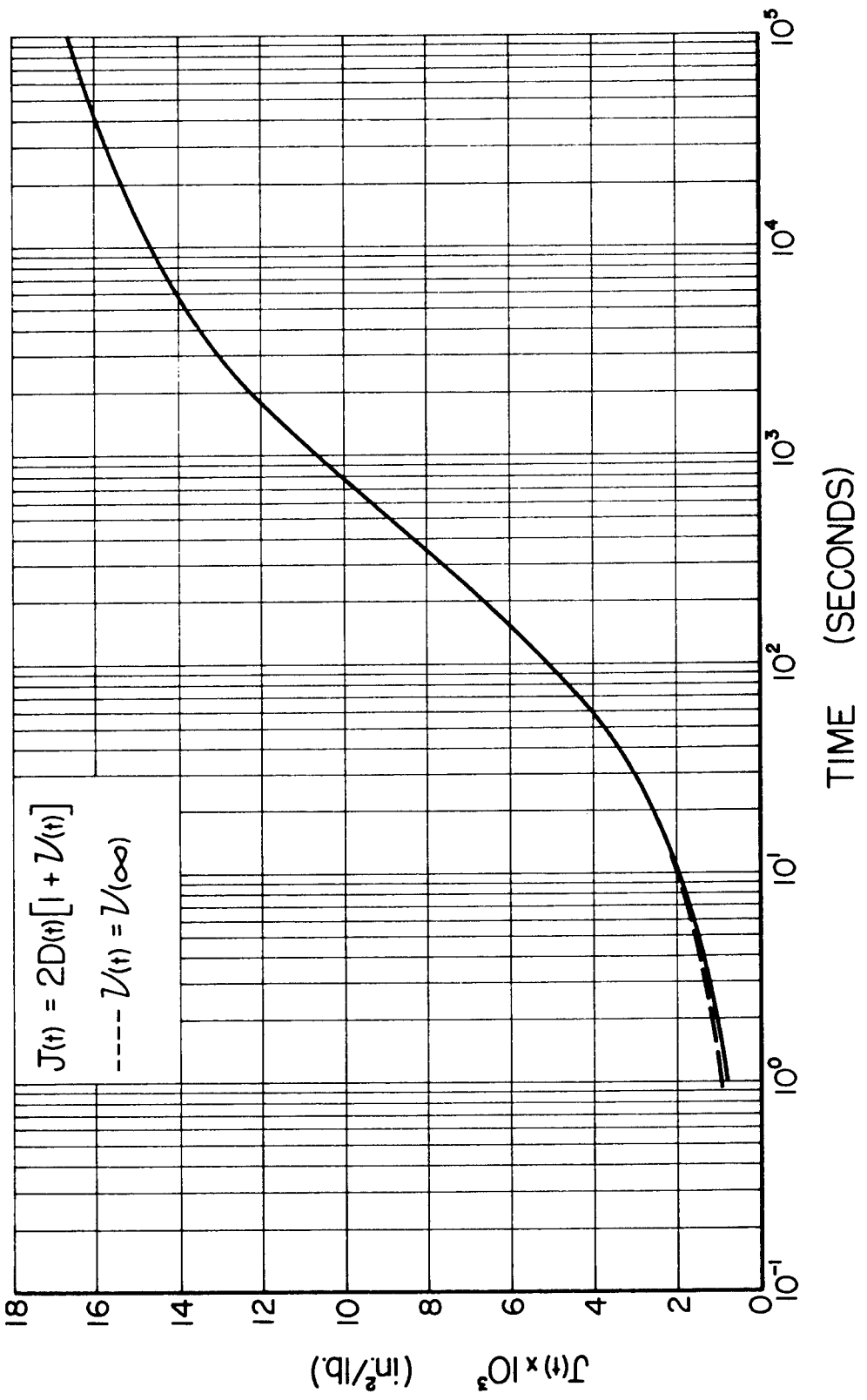

Figure 7. Shear creep compliance (calculated), Mix A.

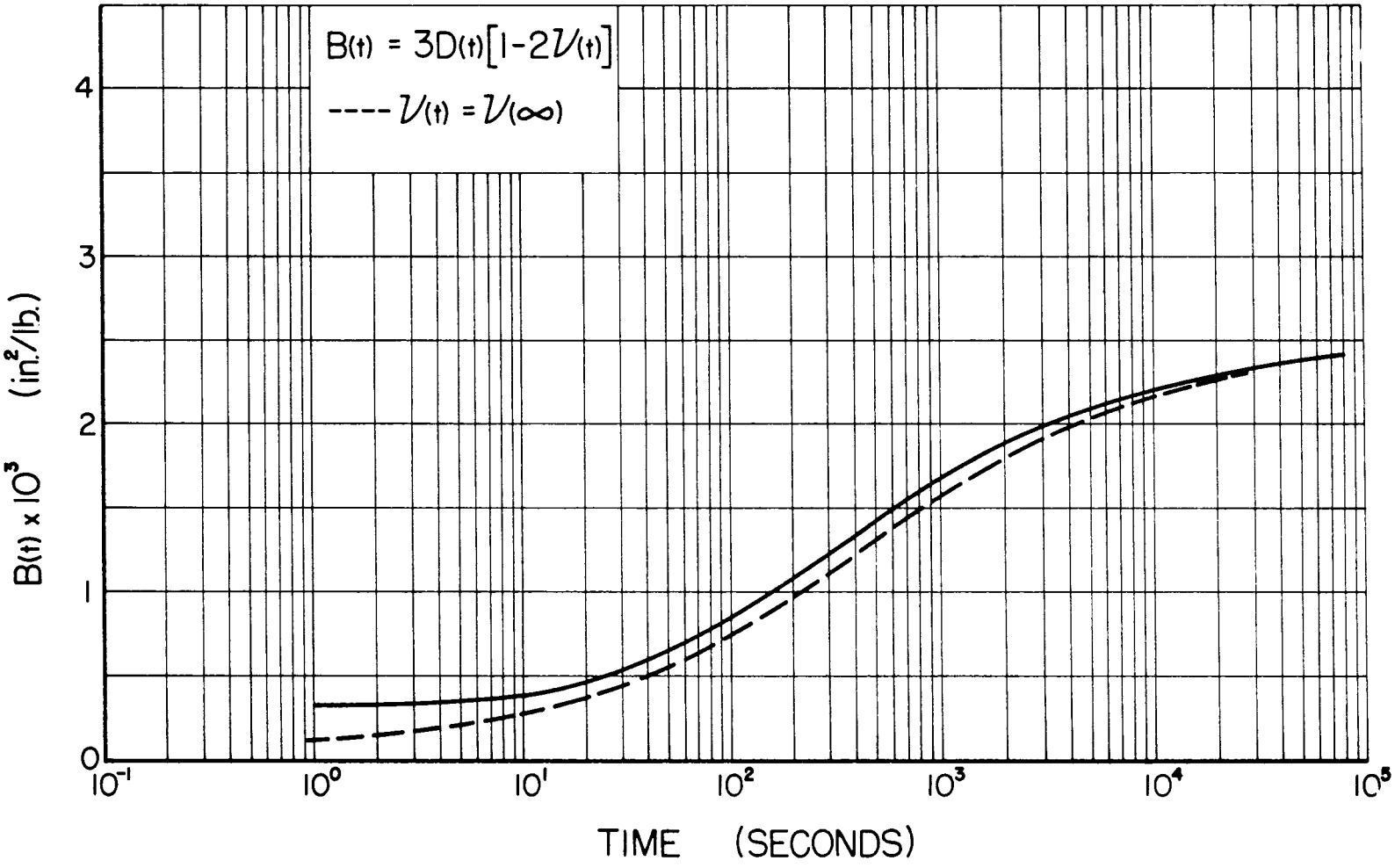

Figure 8. Bulk creep compliance (calculated), Mix A.

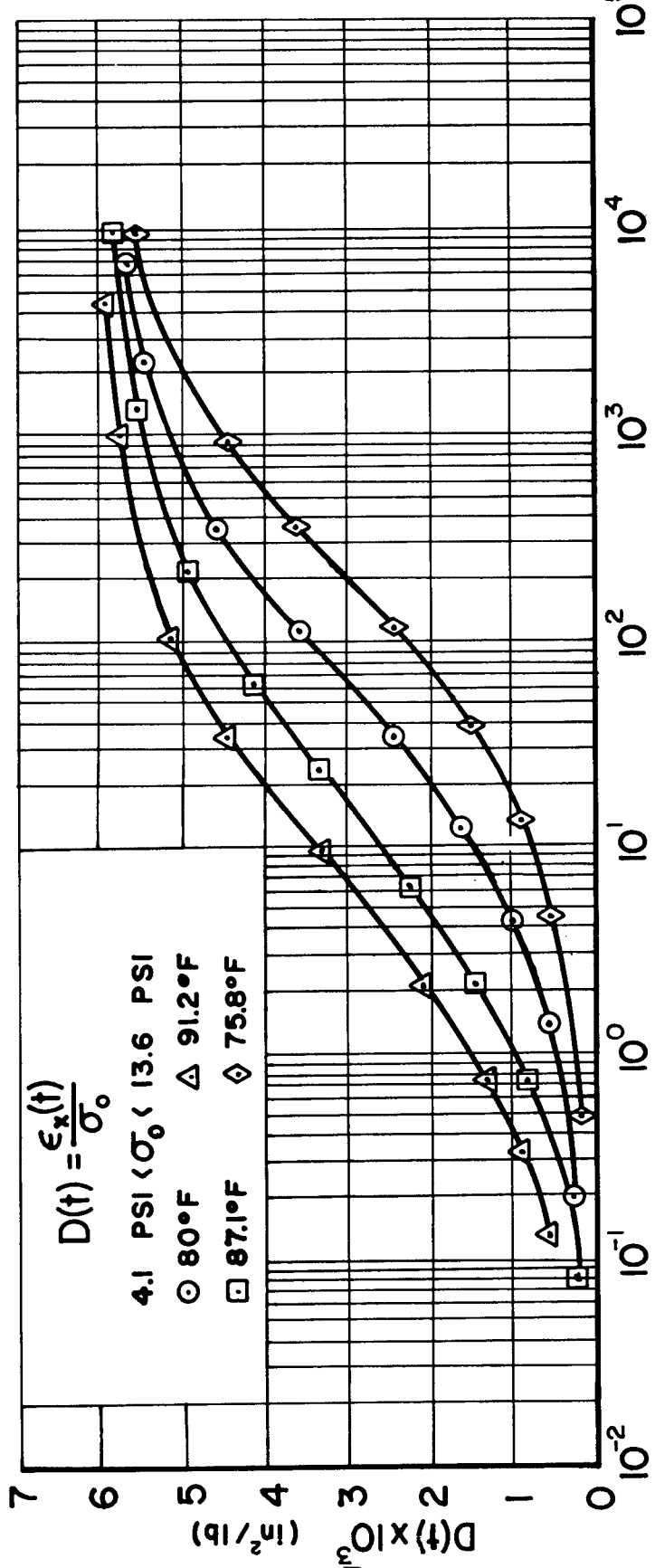

Figure 9. Tensile creep compliance at several temperatures Mix B.

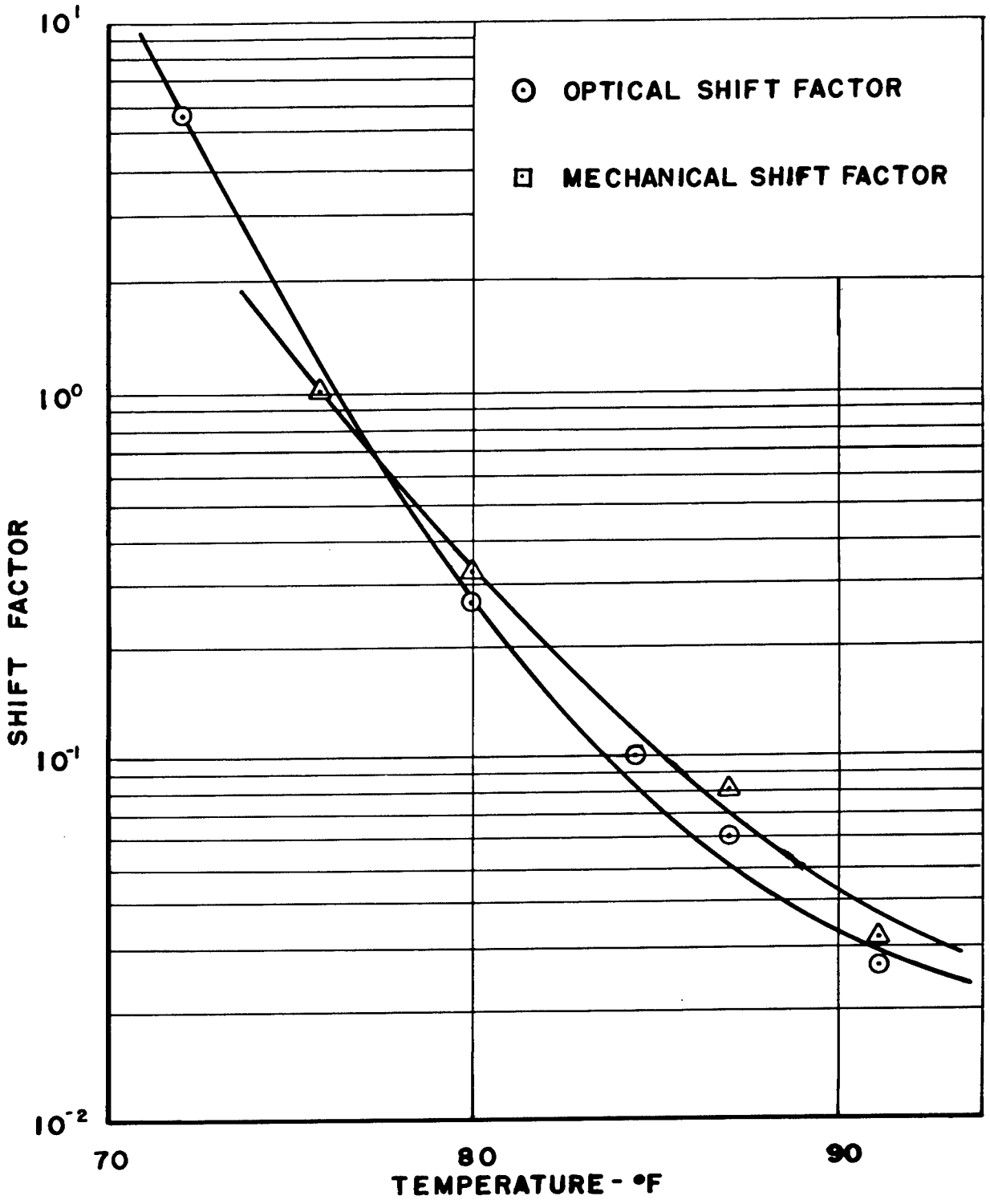

Figure 10. Mechanical and optical shift factors Mix B.

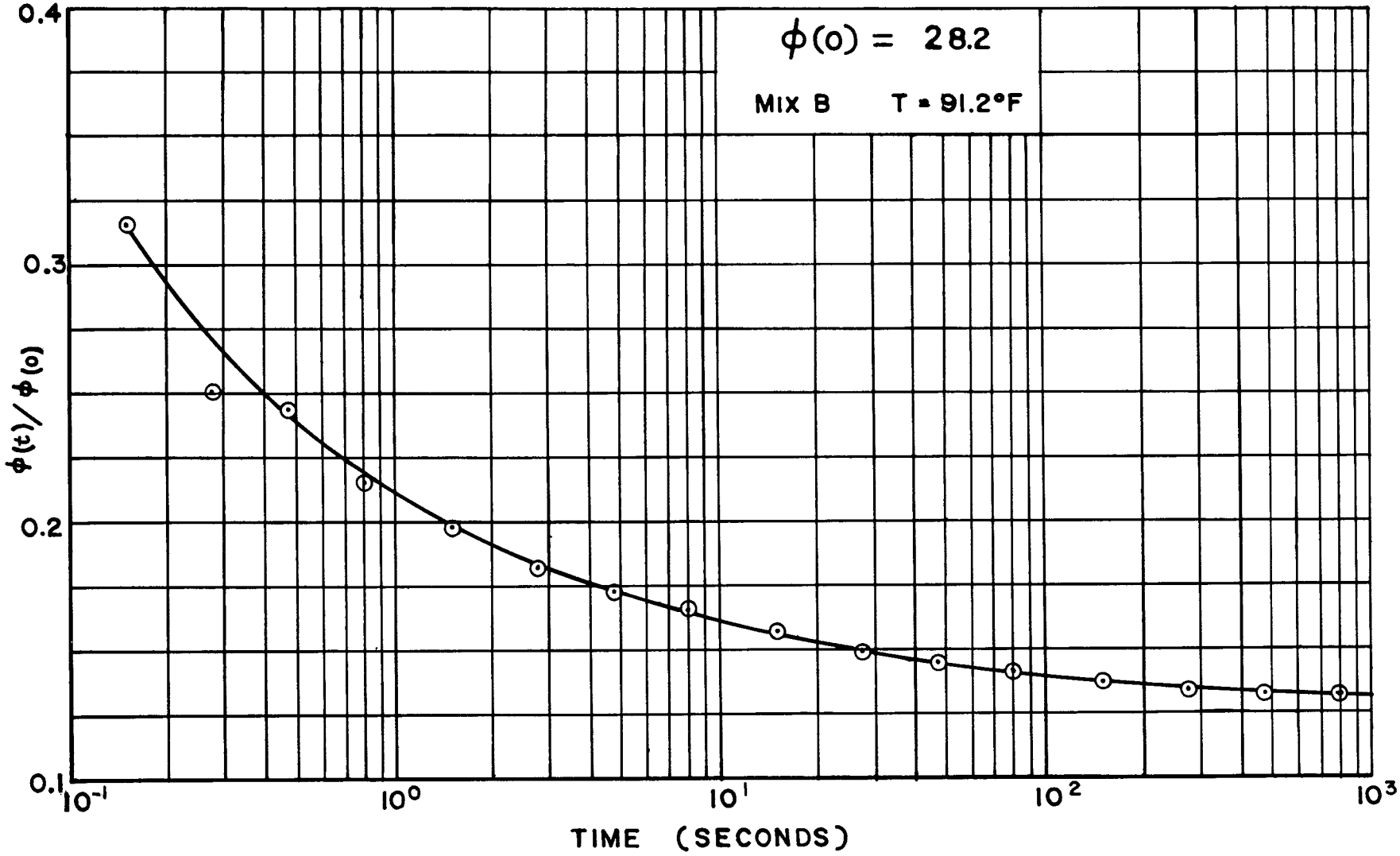

Figure 11. Inverse optical creep function.

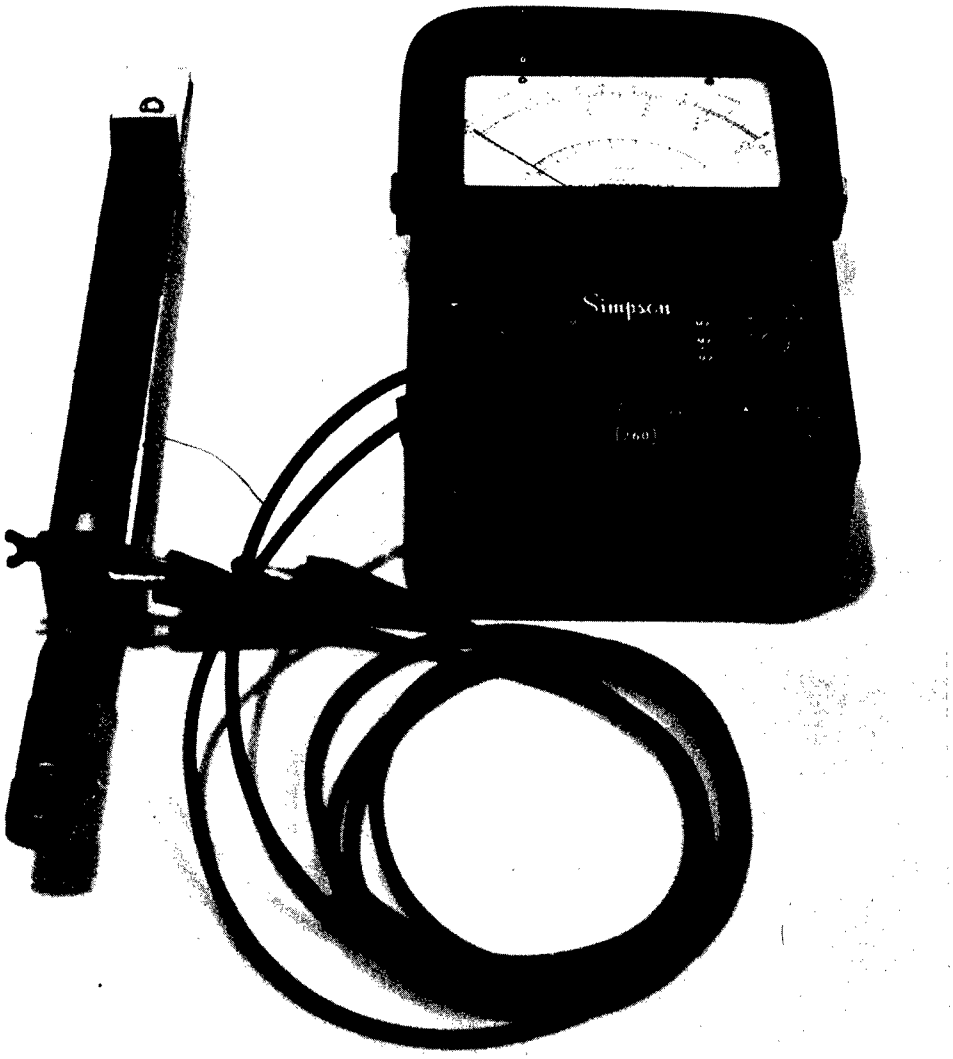

Figure 12. Apparatus for thermal expansion determination.

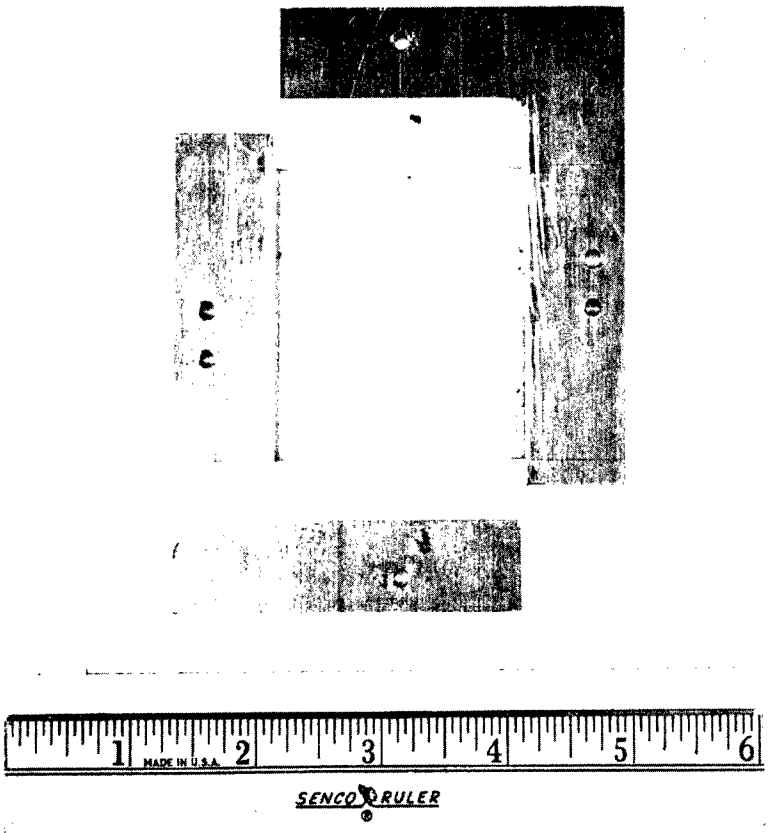

Figure 13. Shear model.

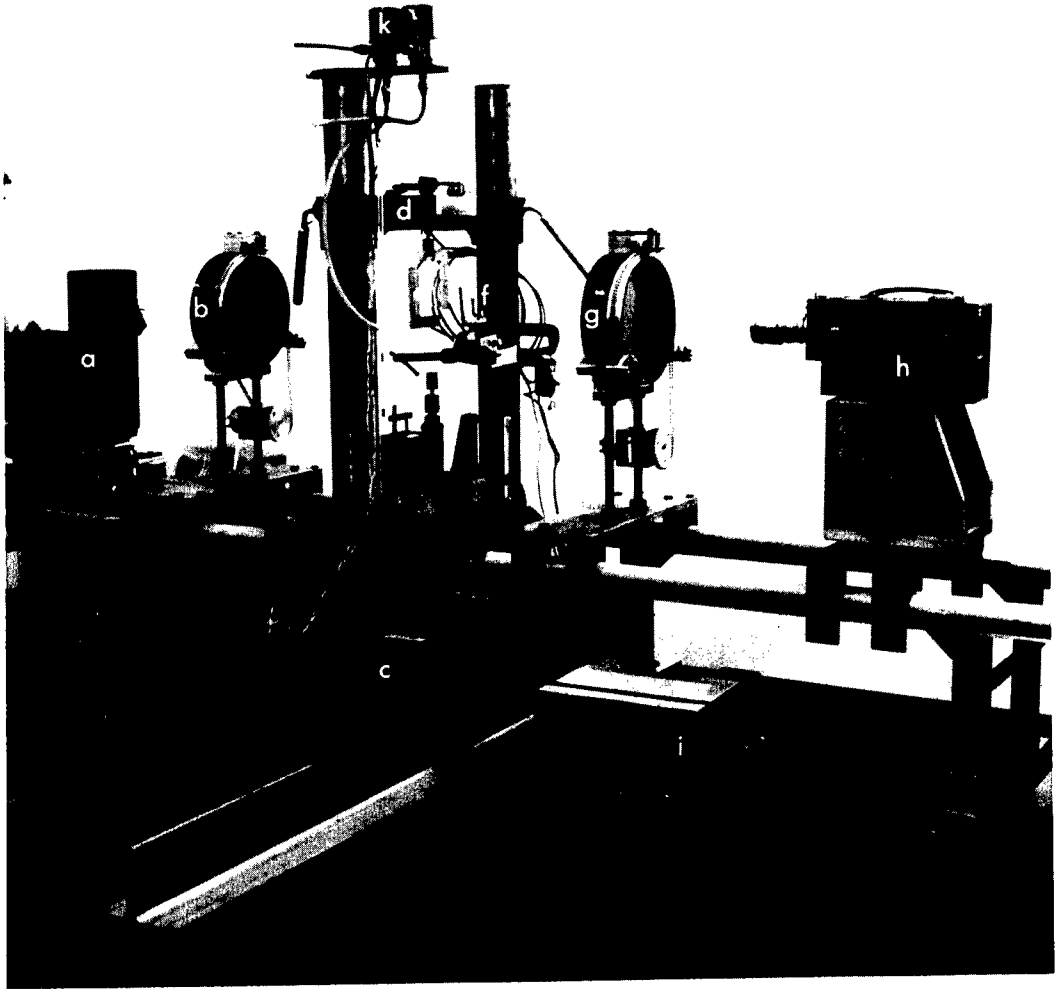

(a) light source, filtered Hg arc
(b) Polaroid, rotating
(c) loading frame
(d) load cell
(e) model
(f) timer and angle indicator
(g) Polaroid, rotating
(h) camera
(i) rotating Polaroid control and power supply
(j) drive solenoids
(k) solenoid valves for pressure loading

Figure 14. Photovisocleastic bench.

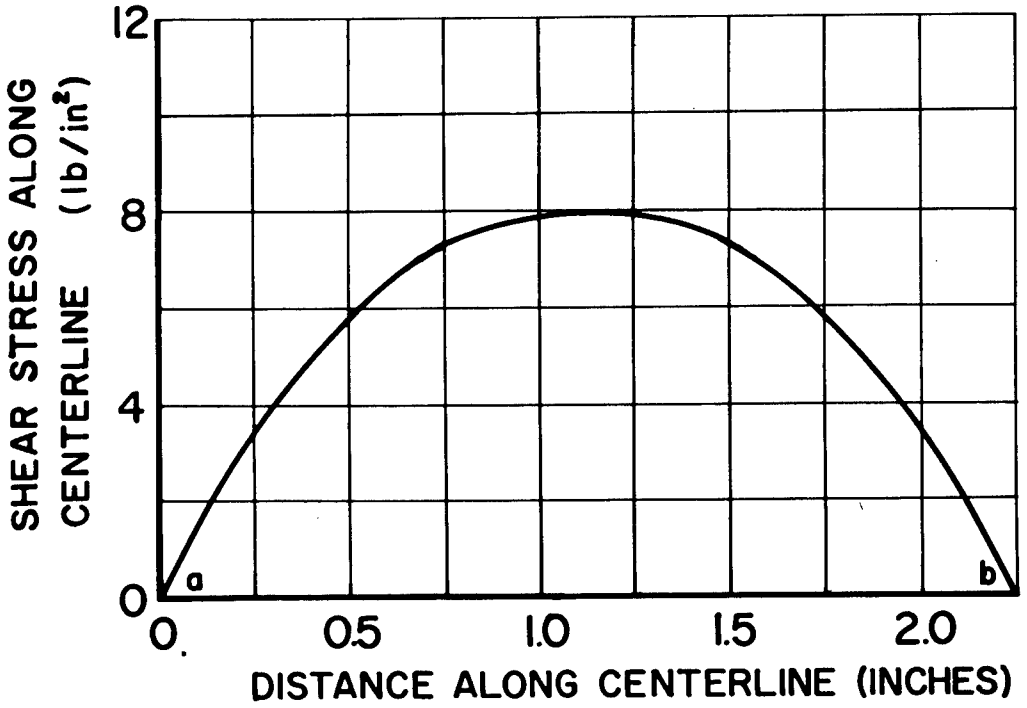

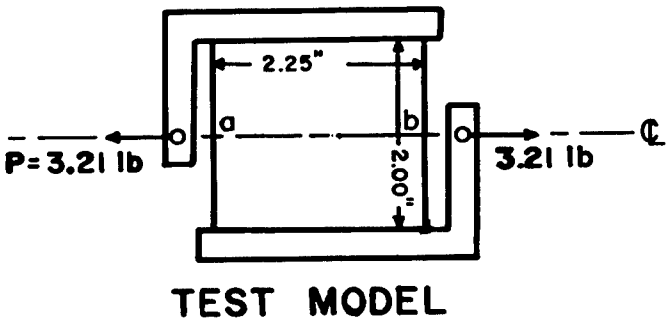

Figure 15. Shear stress distribution.

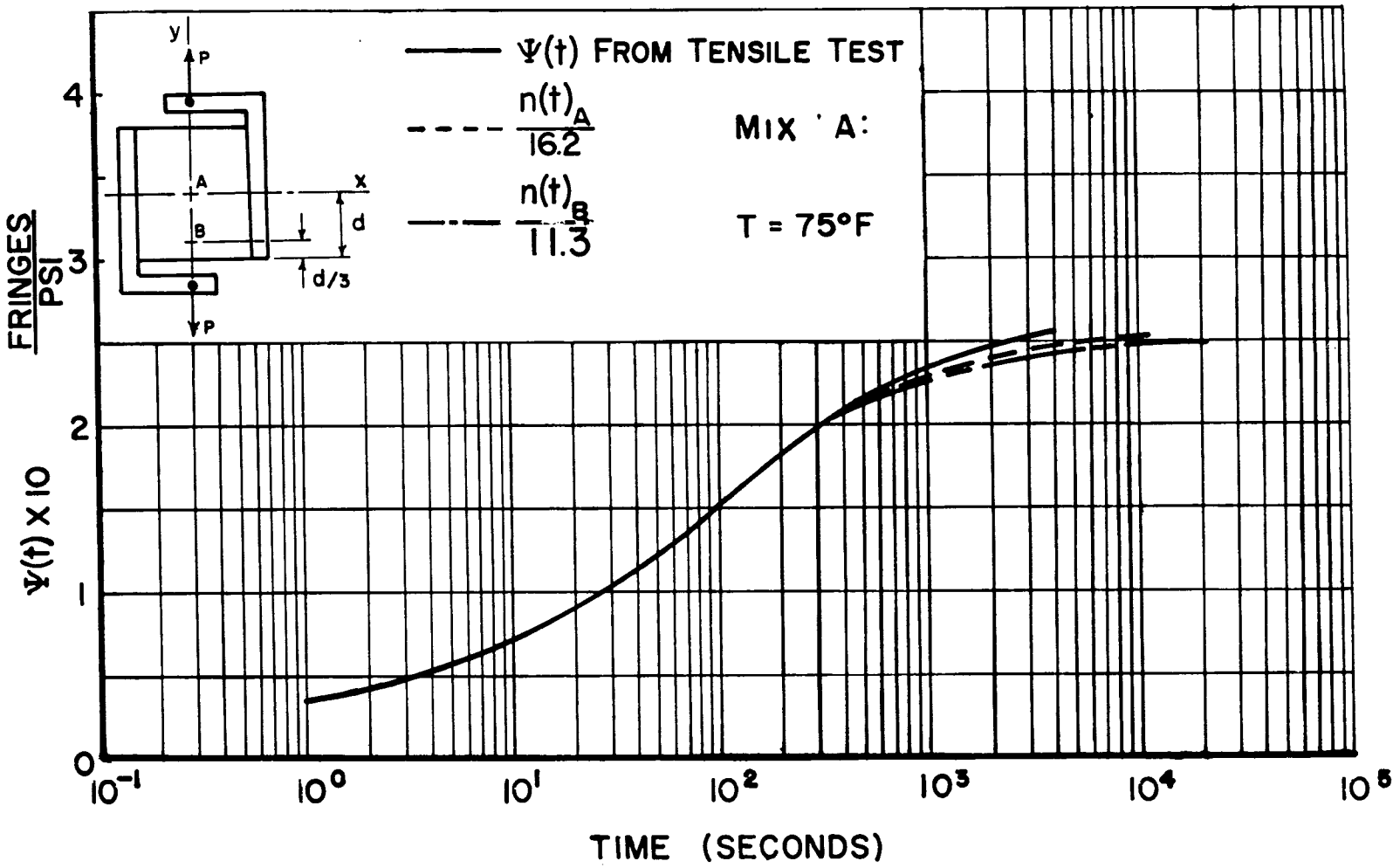

Figure 16. Fringe order in shear test.

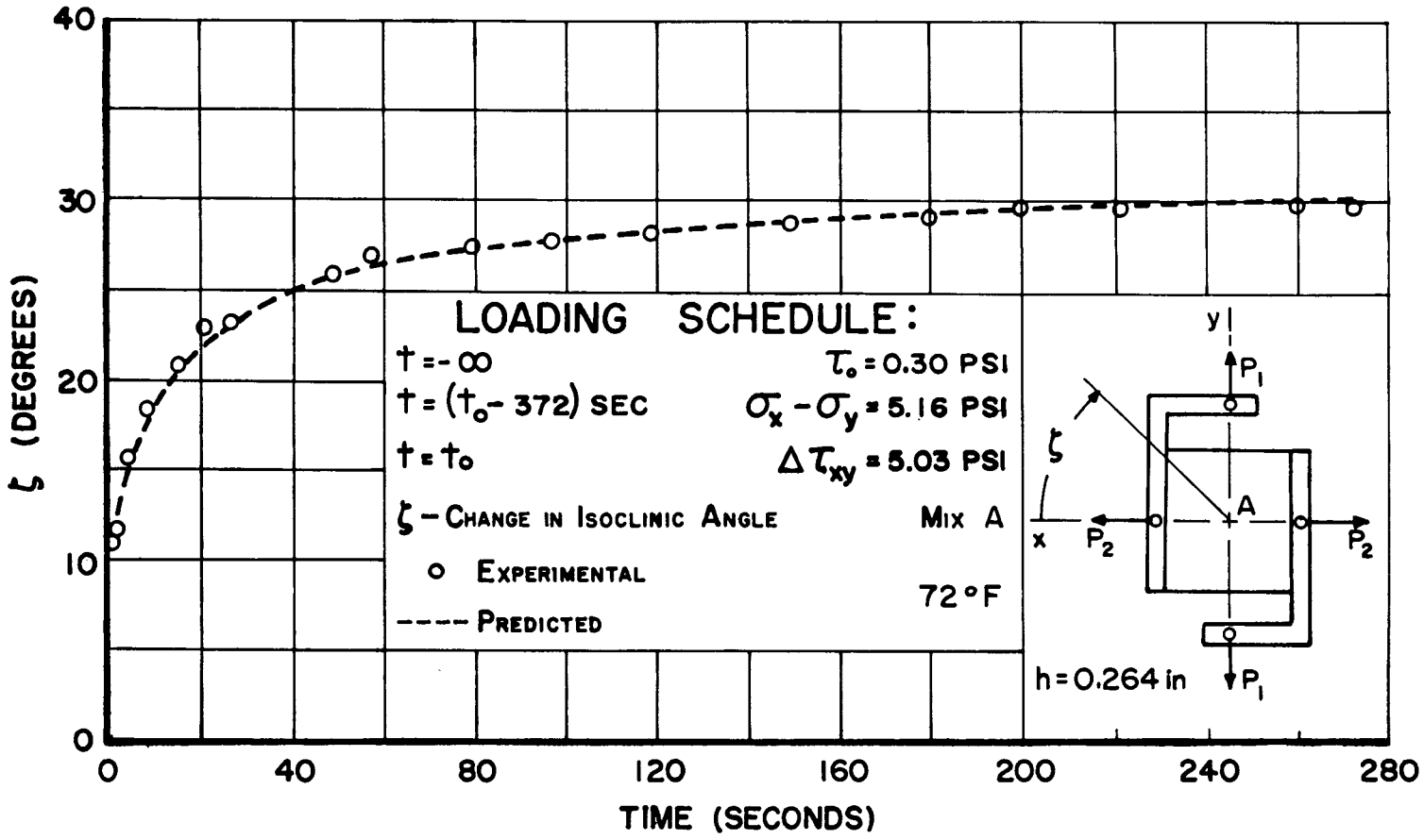

Figure 17. Isoclinic angle in tension-shear test.

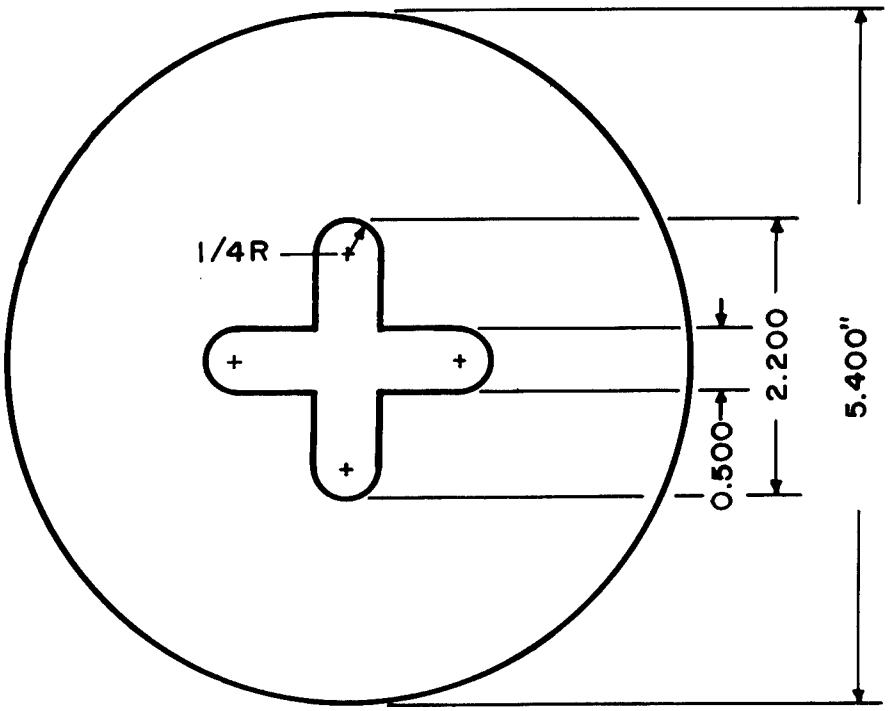

Figure 18. Star grain model.

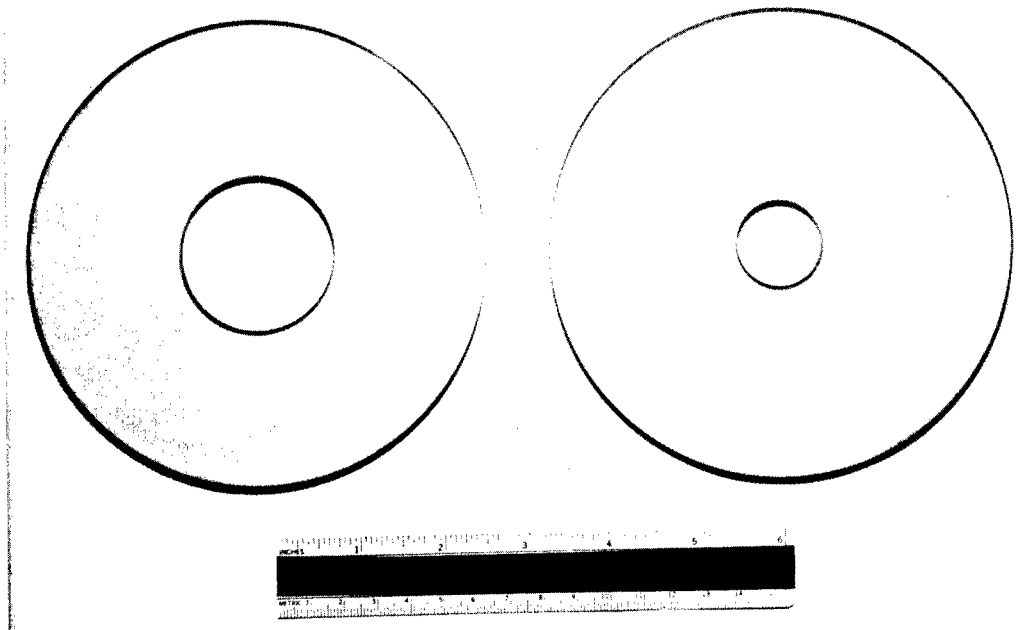

Figure 19. Hysal 4485 calibration specimens for calibrating pressure jig.

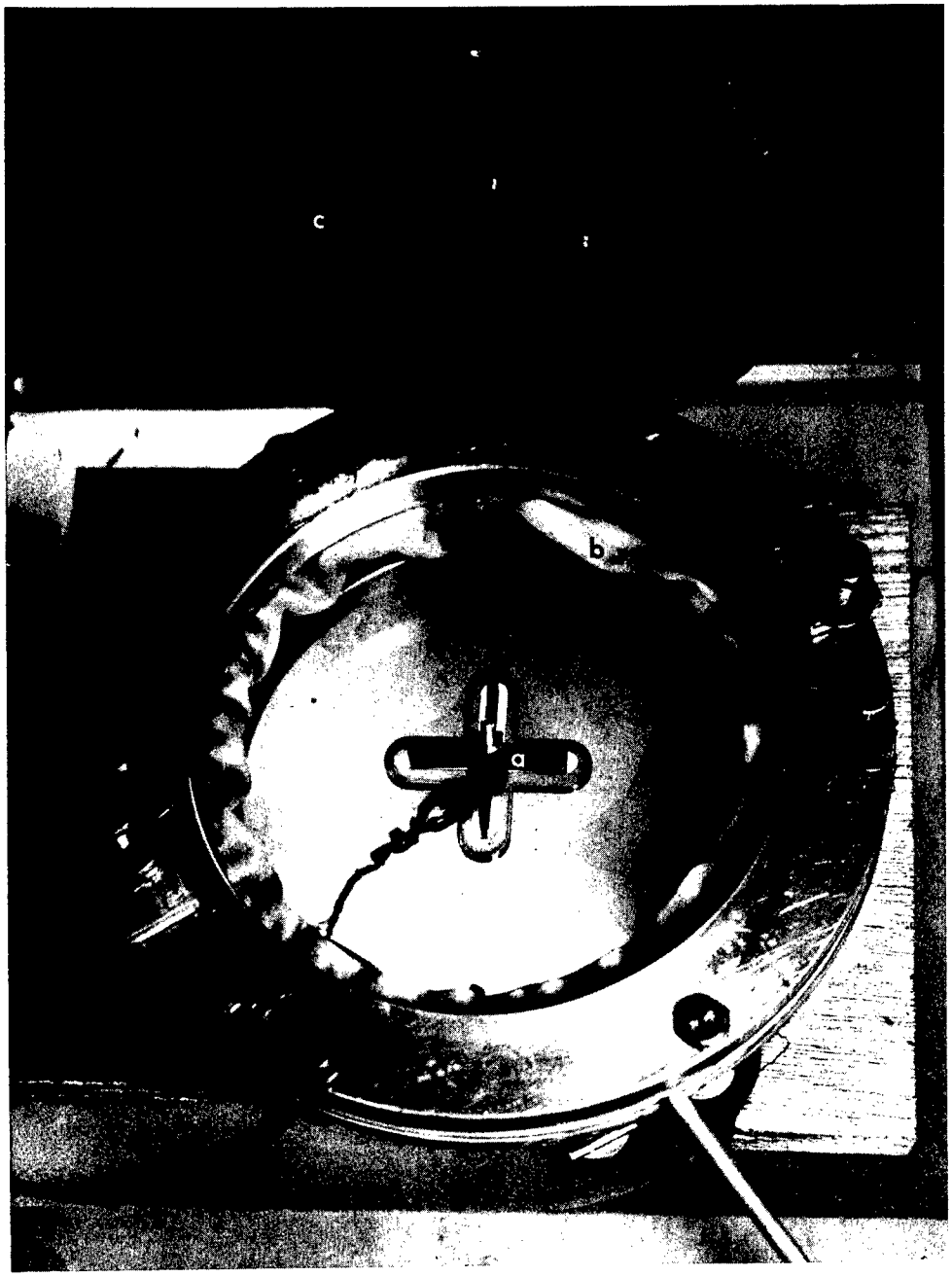

(a) nichrome heater
(b) latex diaphragm
(c) guards, (Polaroid laminated to Plexiglas)

Figure 20. Pressure loading jig (model removed)

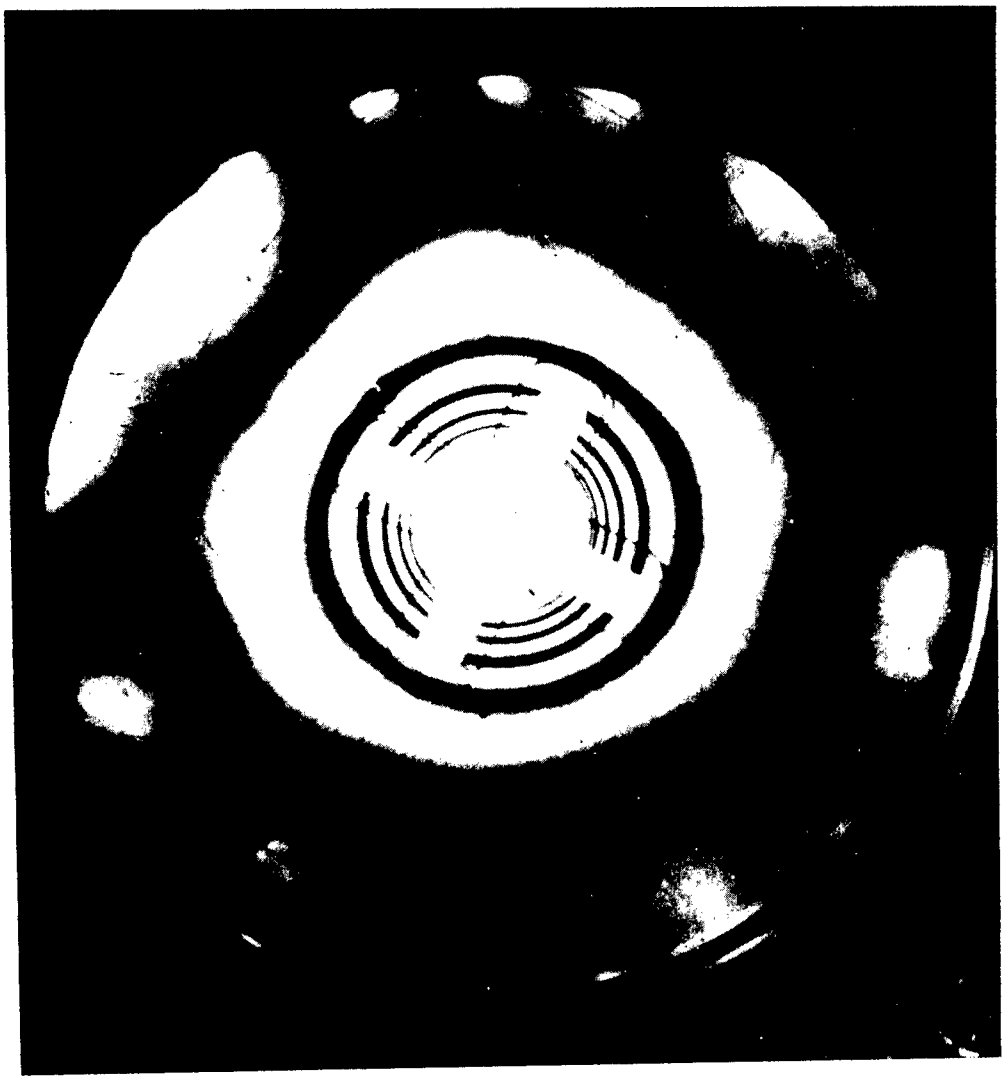

Figure 21. Pressure calibration specimen with circular hole (star cutouts in Polaroid).

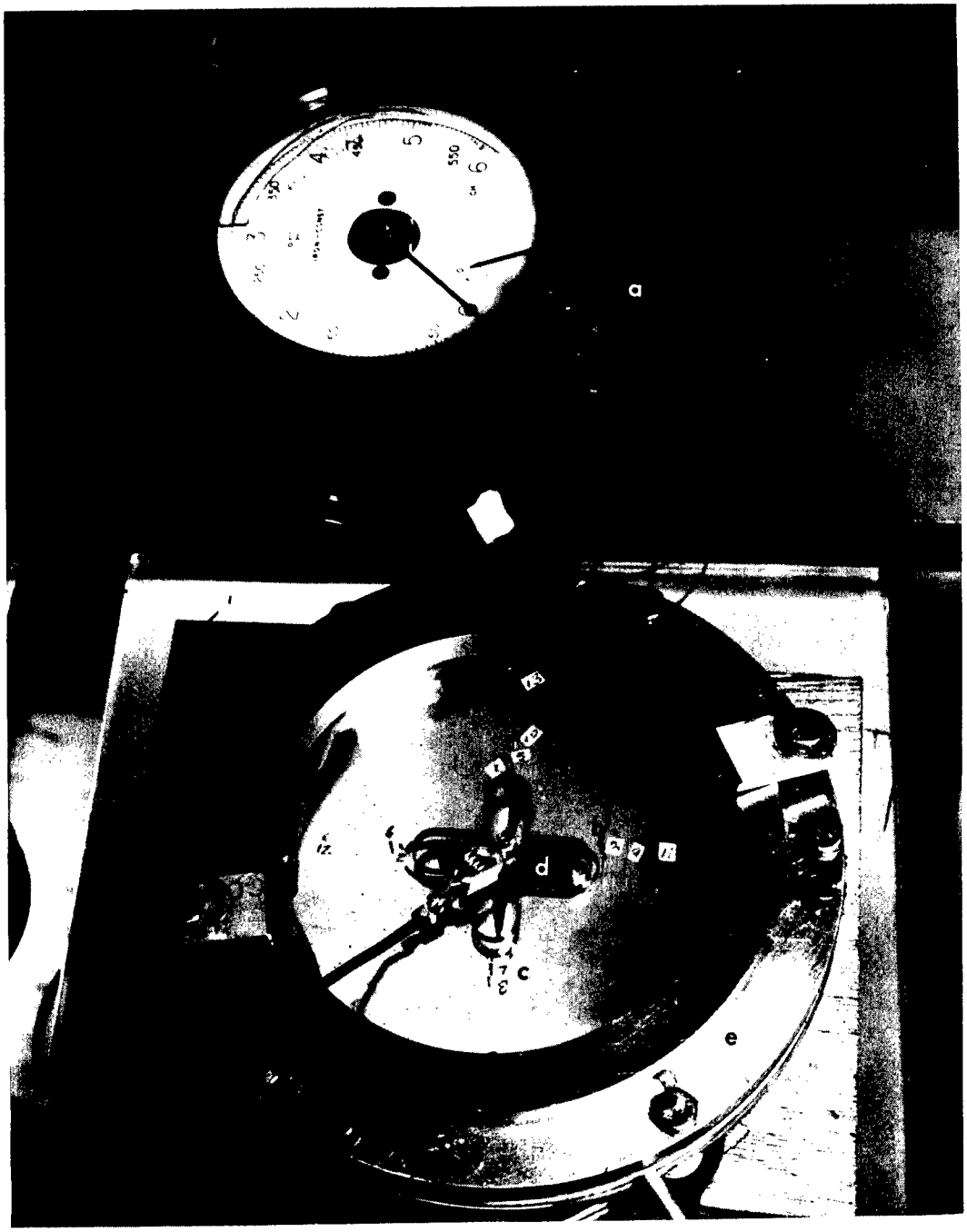

(a) Potentiometer
(b) Thermocouple probe
(c) measuring stations
(d) heater
(e) pressure loading jig

Figure 22. Apparatus for determining temperature distribution.

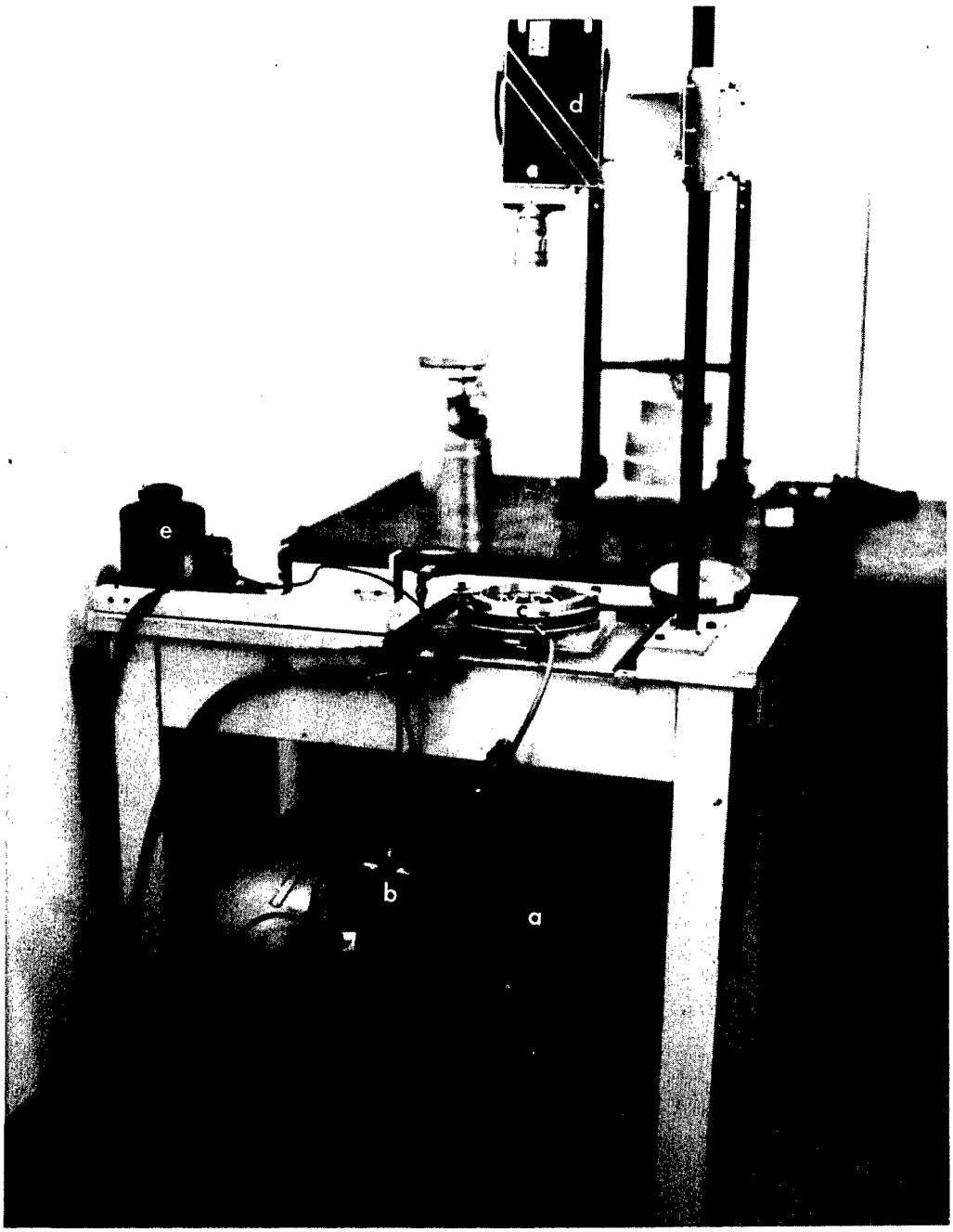

(a) light source, filtered Hg
(b) constant pressure air supply
(c) loading jig (Polaroids incorporated)
(d) camera
(e) heater Variac

Figure 23. Horizontal polariscope for heated model studies.

Figure 24. Isothermal pressurized grain model, 6300 seconds after loading.

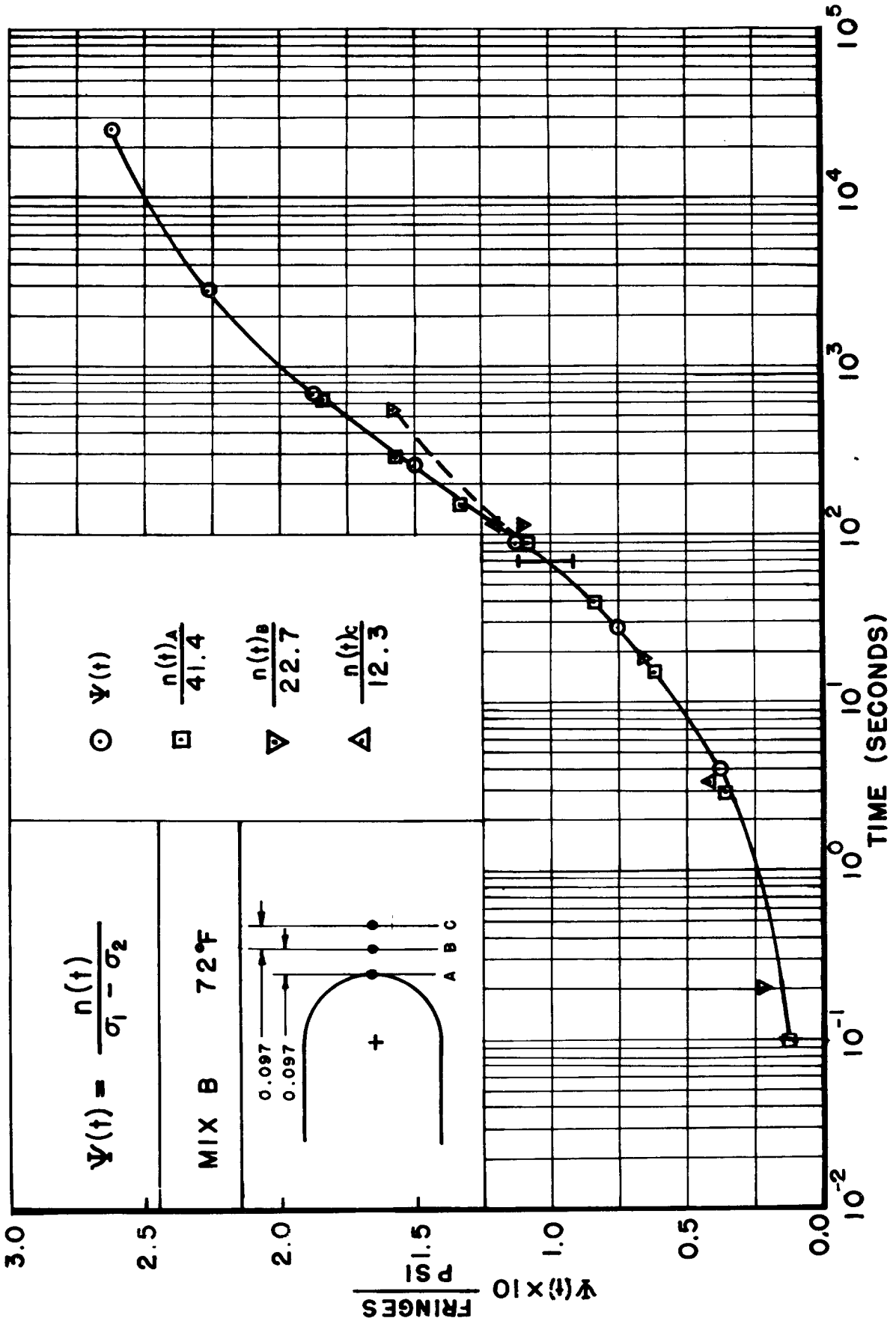

Figure 25. Fringe order at uniform temperature.

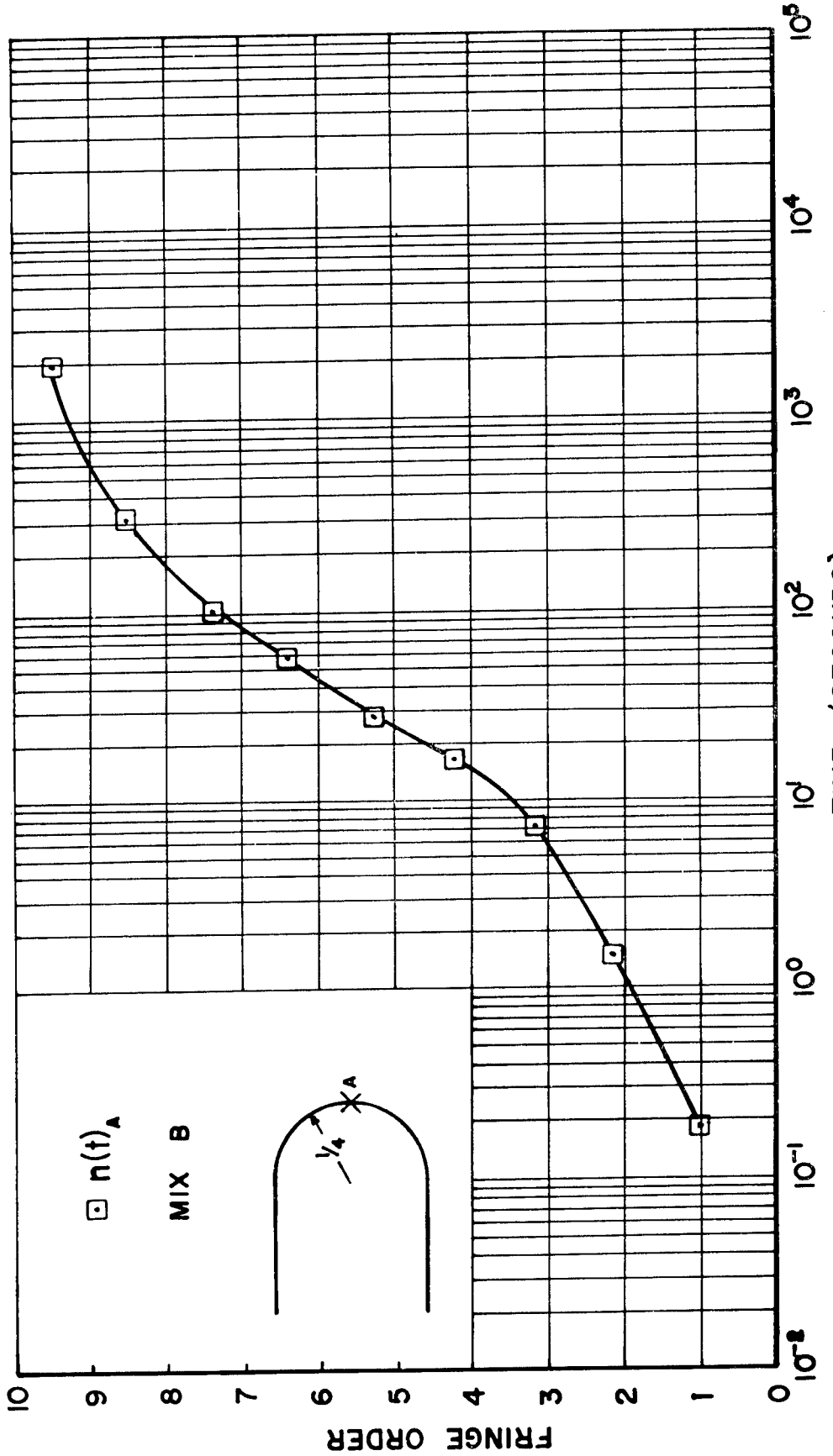

Figure 26. Fringe order, heated model.

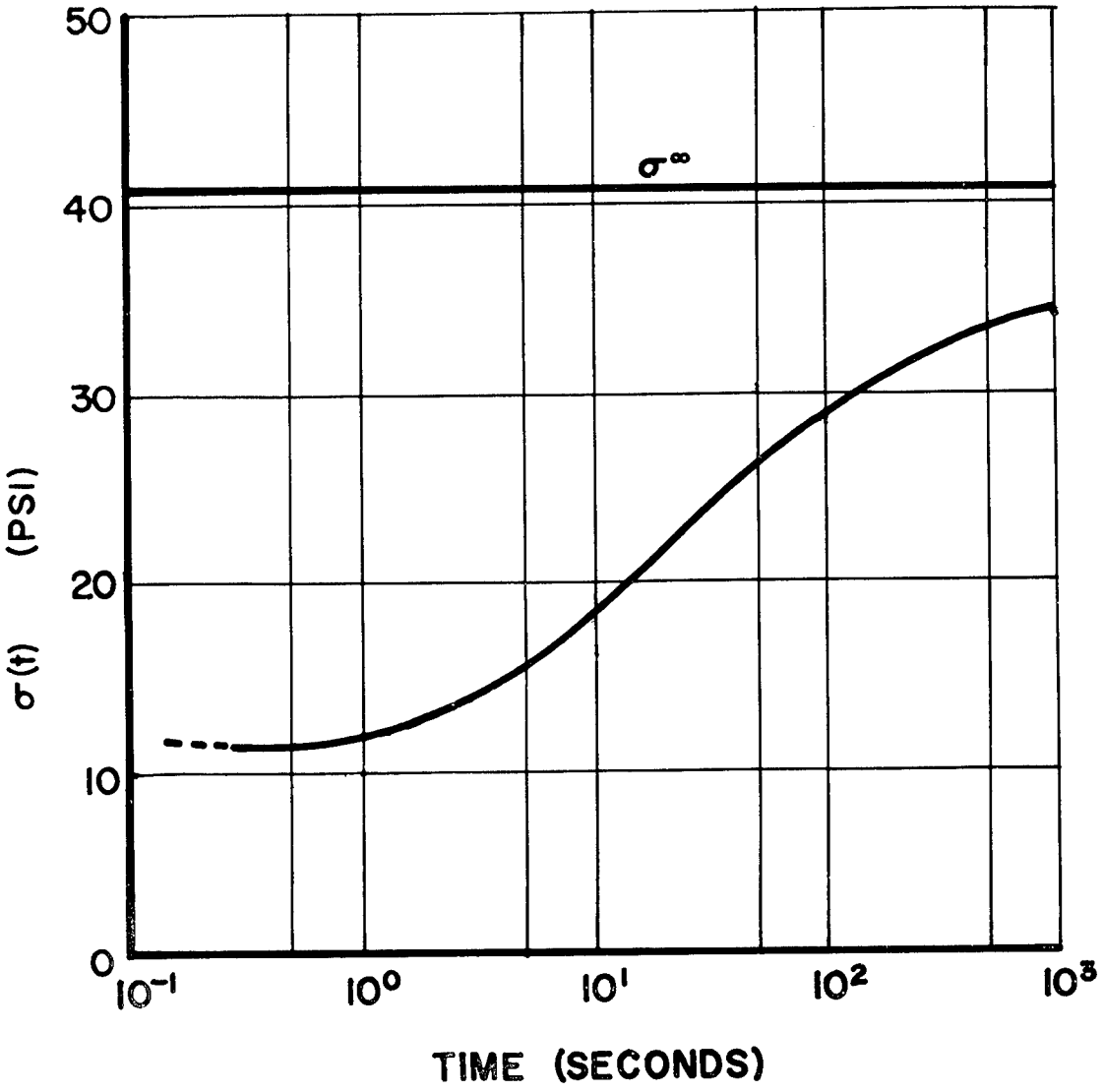

Figure 27. Stress at star root (point A), heated model.

"The aeronautical and space activities of the United States shall be conducted so as to contribute . . . to the expansion of human knowledge of phenomena in the atmosphere and space. The Administration shall provide for the widest practicable and appropriate dissemination of information concerning its activities and the results thereof."

—NATIONAL AERONAUTICS AND SPACE ACT OF 1958

NASA SCIENTIFIC AND TECHNICAL PUBLICATIONS

TECHNICAL REPORTS: Scientific and technical information considered important, complete, and a lasting contribution to existing knowledge.

TECHNICAL NOTES: Information less broad in scope but nevertheless of importance as a contribution to existing knowledge.

TECHNICAL MEMORANDUMS: Information receiving limited distribution because of preliminary data, security classification, or other reasons.

CONTRACTOR REPORTS: Technical information generated in connection with a NASA contract or grant and released under NASA auspices.

TECHNICAL TRANSLATIONS: Information published in a foreign language considered to merit NASA distribution in English.

TECHNICAL REPRINTS: Information derived from NASA activities and initially published in the form of journal articles.

SPECIAL PUBLICATIONS: Information derived from or of value to NASA activities but not necessarily reporting the results of individual NASA-programmed scientific efforts. Publications include conference proceedings, monographs, data compilations, handbooks, sourcebooks, and special bibliographies.

Details on the availability of these publications may be obtained from:

SCIENTIFIC AND TECHNICAL INFORMATION DIVISION

NATIONAL AERONAUTICS AND SPACE ADMINISTRATION

Washington, D.C. 20546